General Disclaimer

One or more of the Following Statements may affect this Document

- This document has been reproduced from the best copy furnished by the organizational source. It is being released in the interest of making available as much information as possible.

- This document may contain data, which exceeds the sheet parameters. It was furnished in this condition by the organizational source and is the best copy available.

- This document may contain tone-on-tone or color graphs, charts and/or pictures, which have been reproduced in black and white.

- This document is paginated as submitted by the original source.

- Portions of this document are not fully legible due to the historical nature of some of the material. However, it is the best reproduction available from the original submission.

NASA CR-170573

(NASA-CR-170573) PRELIMINARY DESIGN OF A 15   N83-34121
M DIAMETER MECHANICALLY SCANNED DEPLOYABLE
OFFSET ANTENNA Final Report (Lockheed
Missiles and Space Co.)   69 p HC A04/MF A01   Unclas
                                CSCL 20N G3/32 36489

Lockheed Missiles & Space Company, Inc.
SUNNYVALE, CALIFORNIA

FINAL REPORT

PRELIMINARY DESIGN OF A 15 M DIAMETER

MECHANICALLY SCANNED DEPLOYABLE

OFFSET ANTENNA

CONTRACT NAS5-26495

Submitted To

NATIONAL AERONAUTICS AND SPACE ADMINISTRATION

GODDARD SPACE FLIGHT CENTER

Greenbelt Road

Greenbelt, Maryland   20771

By

LOCKHEED MISSILES & SPACE COMPANY, INC.

Sunnyvale, California   94086

PREFACE

This report documents the results of Contract NAS5-26495. The preliminary
design of a 15 meter diameter, mechanically scanned, offset rotating, fed
parabolic reflector antenna system is reported and the results of prelim-
inary performance, structural and thermal analyses are presented.

TABLE OF CONTENTS

LIST OF FIGURES

LOCKHEED MISSILES & SPACE COMPANY, INC.

LIST OF FIGURES (Continued)

LIST OF TABLES

1.0 INTRODUCTION

A small 0.2 man year study has been accomplished on the preliminary design
of a 15 meter diameter offset antenna system for application in a mechani-
cally scanned high efficiency multi-frequency radiometer has been accom-
plished. The design activity results, presented in Section 2.0, and the
analytical activity, presented in Section 3.0, succeeded in developing a
mechanical design which is compatible with the design requirements. That
is the mechanical design will provide an extremely high main beam effic-
iency. The effects of thermal distortion and mechanical scan are not sys-
tem drivers.

The basic electrical analysis uncovered a substantial concern. This is
the main beam efficiency effect of off-axis scan of the low frequency
(5.1 GHz and below) beams. As indicated in the report, a simple, ideal
circular feed aperture when scanned off-axis is not able to provide, for
an ideal mechanical system, the desired 90% main beam efficiency. The
results indicate that for the 5.1 GHz frequency the scanned beam effici-
ency will be no greater than 0.83. This can be improved by employing a
larger under-illuminated long focal length aperture for the low frequen-
cies similar to the 11 GHz application or by employing a complex shared
aperture shaping feed and beam forming network. The more complex feed
would bring associated network losses while the larger long focal length
aperture would add significant mechanical impacts.

The results indicate that the desired on-axis main beam efficiency require-
ment of 90% is probably obtainable for all frequencies as is the 90%
scanned beam efficiency at 11 GHz with the significantly longer focal
length system.

1

2.0 SYSTEM DESCRIPTION

2.1 REQUIREMENTS

Established system ground rules require a 15 meter effective circular aperture offset parabolic deployable antenna mechanically scanned at 6 rpm in a conical pattern having a 35° half angle about NADIR. It will be operated on a spacecraft in a 700 km 12:00 sun-synchronous orbit. The antenna shall operate at frequencies of 1.414, 4.3, 5.1 and 11 GHz. The feed shall consist of a 10 horn array for operation at 4.3 GHz and a 5 horn array for operation at 1.4 GHz. The antenna shall be dynamically balanced at the required spin rate. The complete antenna system shall be capable of being launched on a single Space Shuttle flight in a launch volume not greater than 4 m diameter by 7 m long. The stowed configuration structural resonance frequency shall be > 25 Hz, and the scanning resonance frequency shall be > 12 Hz.

2.2 ANTENNA DESCRIPTION

The antenna system chosen to meet these requirements is a 15 m diameter parabolic wrap rib reflector offset fed by a multiple horn array. Stowage requirements are met by mounting the feed and reflector on extendible triangular trusses, and the antenna system is dynamically balanced by counterweights mounted on extendible booms. The complete antenna assembly is depicted in Figures 2.2-1 and 2.2-2, and key ground design features are summarized in Table II-1.

The stowed configuration is shown in Figure 2.2-2 and the deployment sequence is described by Figure 2.2-3. Deployment is accomplished by first rotating the reflector mast cannister as shown in Step b. The reflector

2
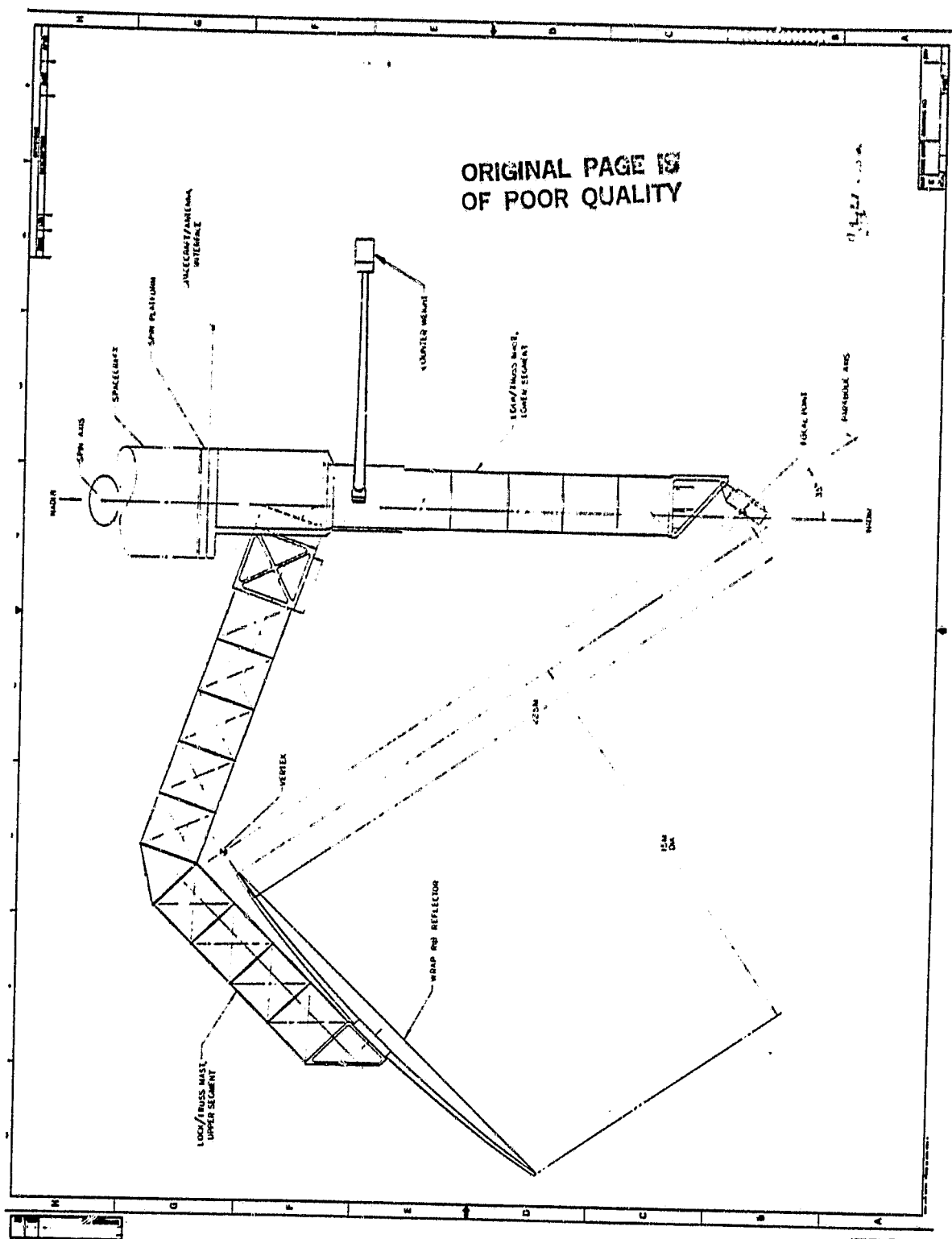
Figure 2.2-1 MSDA Configuration

3

ORIGINAL PAGE IS
OF POOR QUALITY

Figure 2.2-2 MSDA Configuration

4

Table II-1 Antenna System Configuration

PARAMETER	DESIGN	REQUIREMENT
APERTURE DIA (m)	15	15
ARRANGEMENT	OFFSET PARABOLIC REFLECTOR	OFFSET PARABOLIC REFLECTOR
SCANNING	MECHANICAL 70° CONE	MECHANICAL 70° CONE
BEAM EFFICIENCY	91% (On Axis)	90%
FREQUENCY (GHz)	1.414	1.414
BANDWIDTH (MHz)	28	28
NO. OF BEAMS IN TRACK	3	3
FREQUENCY (GHz)	4.3	4.3
BANDWIDTH (MHz)	200	200
NO. OF BEAMS IN TRACK	10	10
FREQUENCY (GHz)	5.1	5.1
BANDWIDTH (MHz)	100	100
NO. OF BEAMS IN TRACK	12	12
FREQUENCY (GHz)	11	11
BANDWIDTH (MHz)	100	100
NO. OF BEAMS IN TRACK	10	10
NO. OF REFLECTOR RIBS	30	–
MASS	1045 Kg	–
INERTIA		
I_{xY}	241,000 Kg-m^2	–
I_{xZ}	241,000 Kg-m^2	–
I_{xY}	253,000 Kg-m^2	–
ANGULAR MOMENTUM	158,965 $\frac{kg\text{-}m^2}{sec}$	–

Figure 2.2-3 MSDA Deployment Sequence

a) Stowed

b) Reflector Mast
Cannister Rotated

c) Reflector Mast
Deployed

d) Counterweight and Feed
Booms Deployed

e) Reflector Deployed

6

mast is then extended as shown in Step c. The counterweight booms are extended next, the feed mast is extended, and the feed assembly rotated to its deployed position. Finally, the 15 meter reflector is unfurled to complete the system deployment. The MSDA is then ready for spin up to its 6 rpm operating rotation speed.

2.3 REFLECTOR DESCRIPTION

The reflector concept chosen is based on flight proven designs, some of which are depicted in Figure 2.3-1.
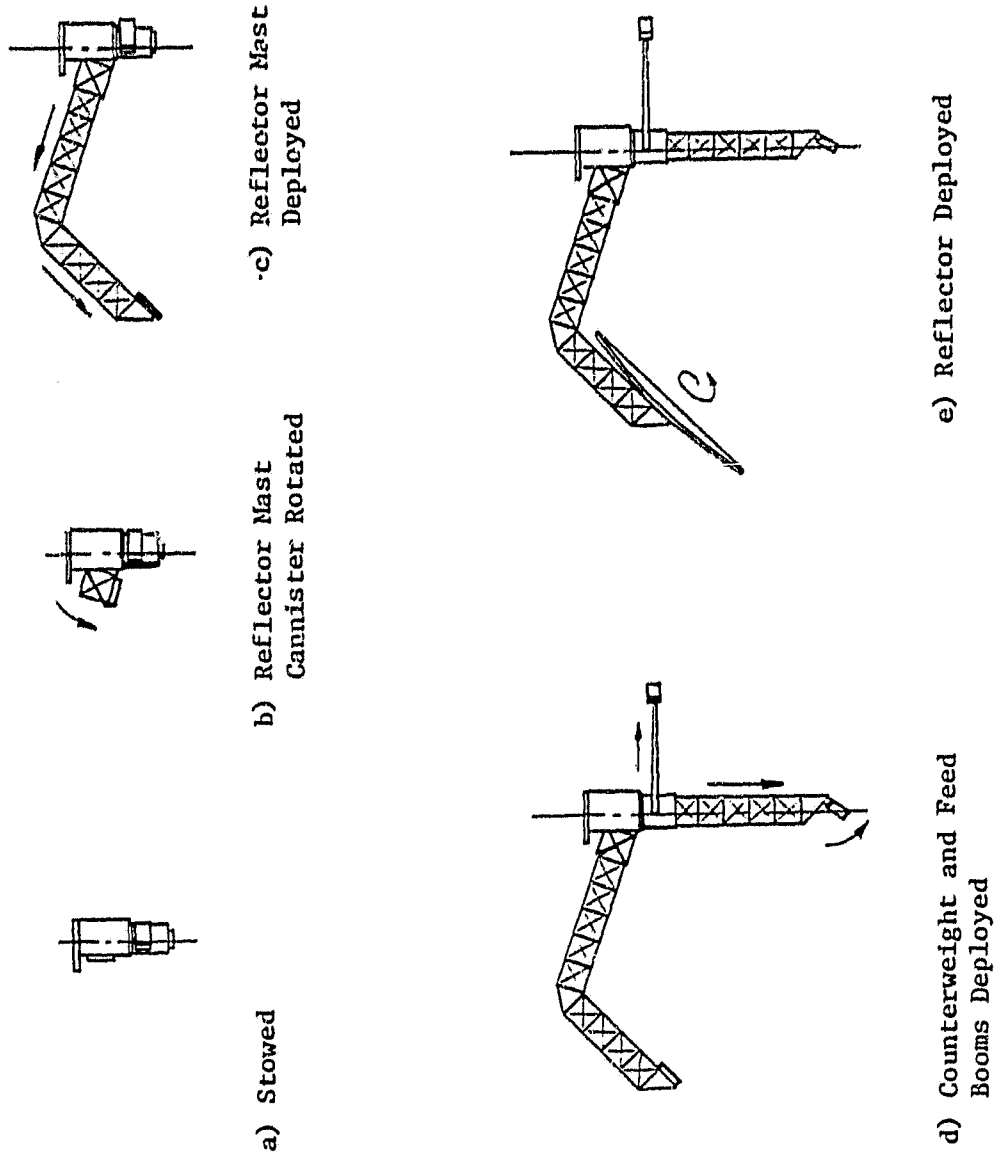
The wrap rib concept first conceived in 1963 was demonstrated at 9.2 meters and 8.3 GHz in 1974 aboard the ATS-6. LMSC recognized at about the same time the future needs for larger apertures operating at higher frequencies. Development of graphite epoxy technologies, mesh surface technology, reflector motor deployment technology, and high precision, repeatable reflector deployment mechanism technologies were initiated and pursued.

A product of these programs was the realization of the critical elements of two designs for 15 meter reflectors; both using G/E technology. These designs (Figure 2.3-2 and 2.3-3), while both generically wrap rib reflectors, differ in the technology development they were intended to provide.

The free deployment reflector, Figure 2.3-2, designed to operate at 12.5 GHz, was developed to provide a very lightweight medium diameter (less than 20 m) system. The hardware depicted in Figure 2.3-3 was designed to ascertain the limits to which G/E technology could be extended. The requirements were to develop the highest stiffness to weight ratio achievable. This reflector, originally intended to support a Shuttle Experimental Mission, was a predecessor model for extremely large apertures. This hardware became the basis for the design of the NASA Large Space Systems Technology 55 meter offset reflector (see Figure 2.3-4) currently

7

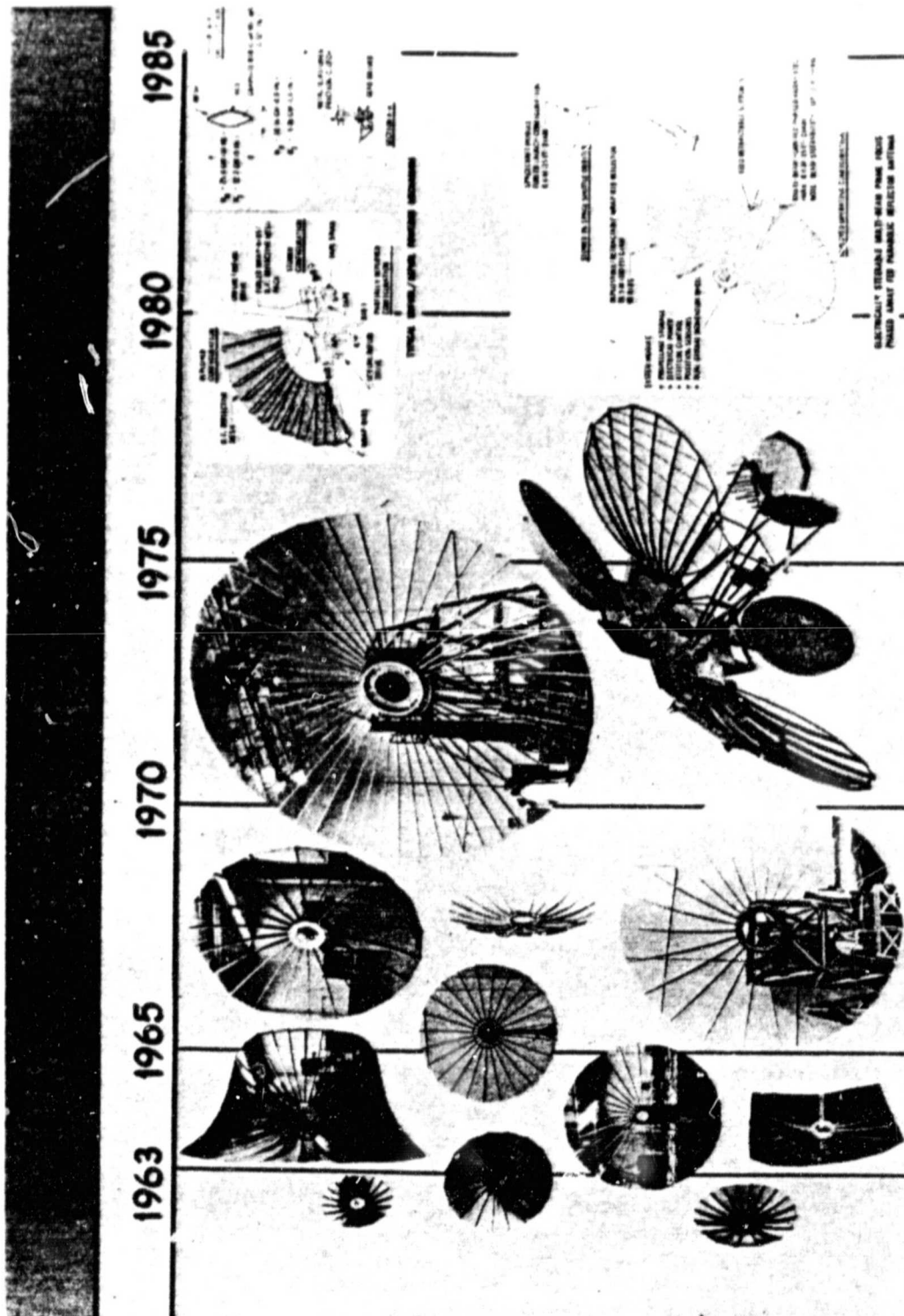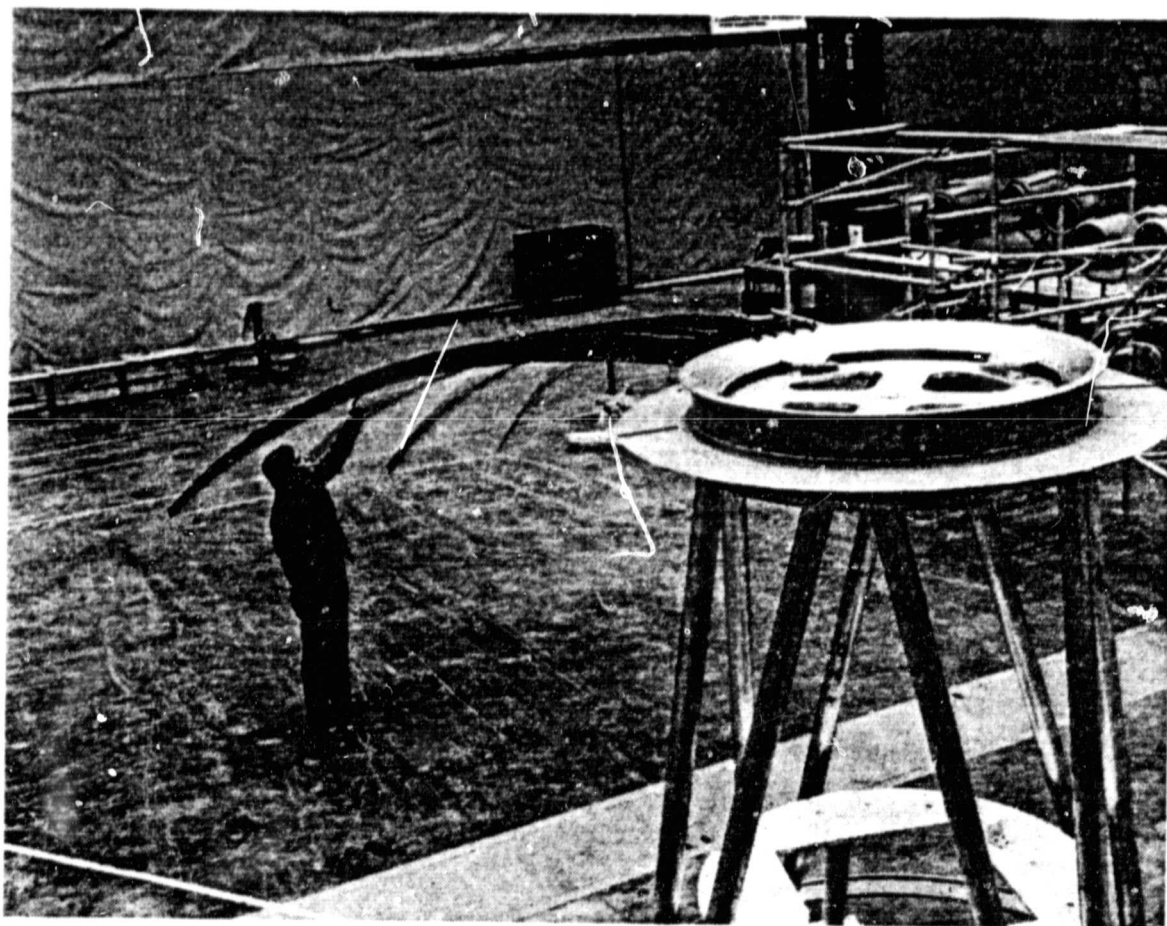Figure 2.3-1 Wrap Rib Reflector Development History
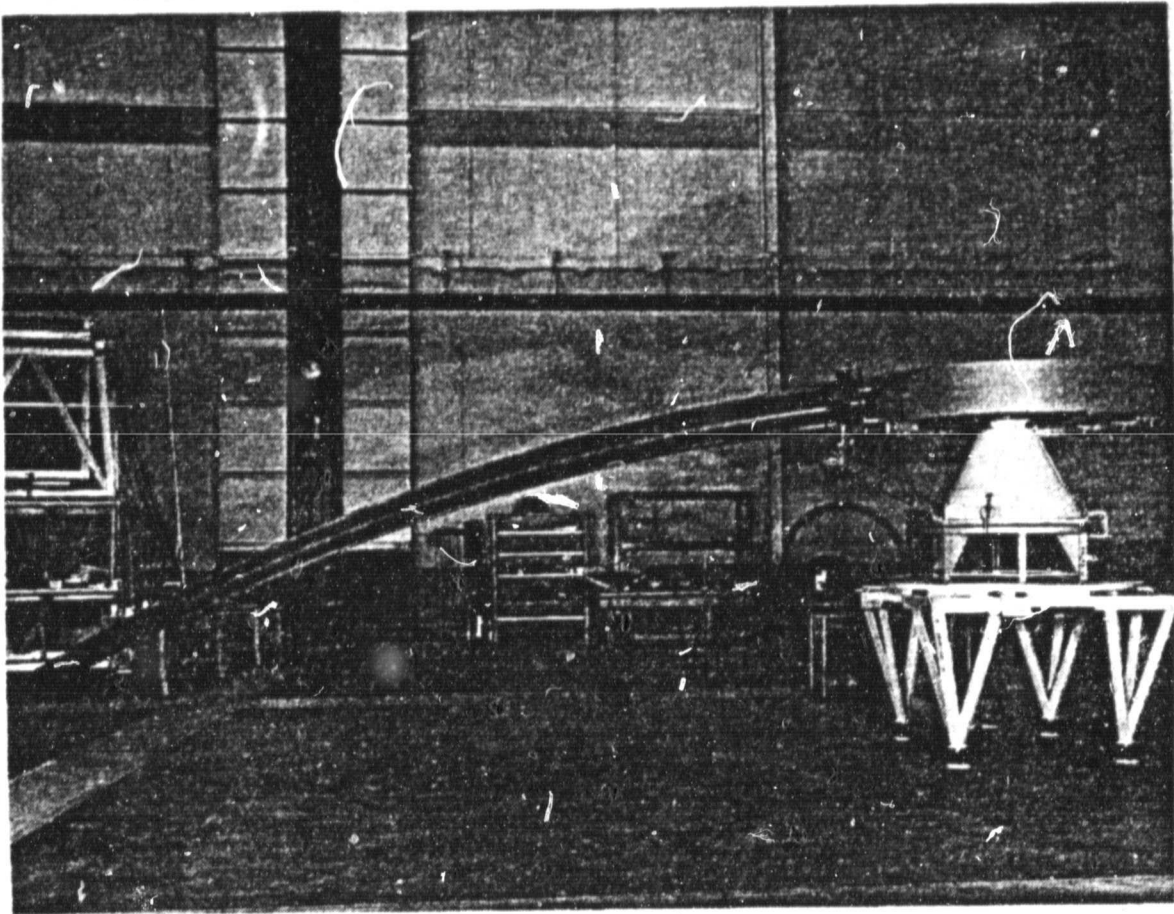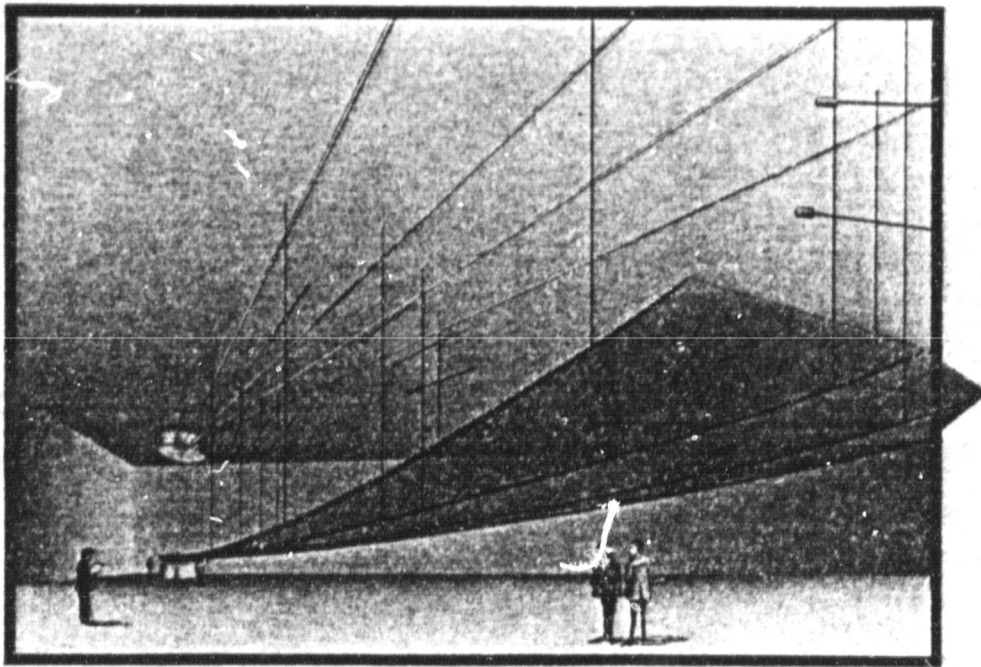
8

Figure 2.3-2 15 m Free Deployment Reflector Segment

9

Figure 2.3-3 15 m Motor Deployed Reflector Rib

10

Ground Test of 55 Meter Reflector

Figure 2.3-4   55 Meter Reflector Segment

11

being developed at LMSC under the auspicies of the Jet Propulsion Laboratory (JPL) and funded by the NASA Langley Research Center. The analysis techniques, design approaches, tooling requirements, and fabrication techniques for this reflector are all directly applicable to the MSDA reflector.

The wrap rib reflector consists of a number (variable) of radial ribs or beams which are cantilevered from a central hub structure. In an offset reflector, this hub is at the center of the offset section. Each of the ribs is attached to this hub through hinges. This radial spoke system provides the support for the reflective surface. The ribs are fabricated with appropriate contours to form the desired parabolic shape. Reflective, pie shaped, gores of a flexible membrane material (mesh) are attached directly to the ribs.

The rib cross section and material are chosen to permit the elastic buckling of the ribs. This allows them to be wrapped around the hub, spiral fashion, in the ascent (stowed) package configuration. In the stowing process, the ribs and attached reflective surface are rotated about the hinges until the ribs are tangent to the hub. After this rotation, the ribs are elastically buckled and wrapped into the receiving container.

The elastic energy stored in the wrapped ribs is sufficient to accomplish deployment of reflectors in this 15 m size range. A motor drive system controls the deployment speed allowing a slow, fully reversible deployment event.

Graphite epoxy was chosen as the rib material due to the inherently low coefficient of thermal expansion that can be achieved. The particular material composition and orientation selected is the Fiberite Company 0.250 mm. HMS/34 tape in a (0°/90°/90°/0°) laminate. The properties of these lamina materials and the resulting composite laminate are listed in Table II-2. The cross section designed for this rib is shown in Figure 2.3-5, and its key design parameters are shown in Table II-3.

12

Table II-2 Material Properties of Layup Configurations

PARAMETER	HMS/HMS/HMS $(0/90_2/0)$
Young's Modulus (msi)	14.0
Shear Modulus (msi)	0.60
Thermal Coefficient of Expansion $(x\ 10^{-6}/°F)$	0.1
Ultimate Tensile Strength (ksi)	57.0
Ultimate Compressive Strength (ksi)	51.0
Thermal Conductivity (Btu/hr-ft-°F)	13.6

Table II-3 Rib Parameters*

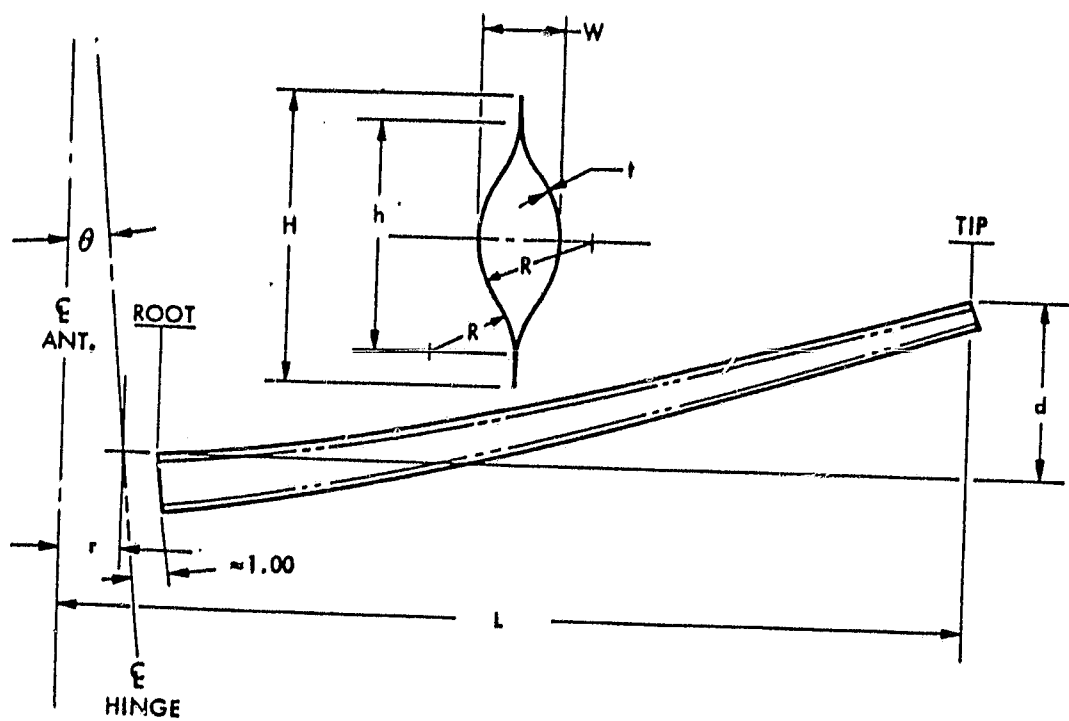| PARAMETER	VALUE
Rib Type	Lenticular
Height (H) (Root)	178 mm
(tip)	50 mm
Width (W) (Root)	38 mm
(tip)	13 mm
Forming Radius (R)	68.7 mm
Length (L)	7.5 m
Thickness (T)	.5 mm
Hub Radius (r)	1.46 m

*See Figure 2.3.5 for physical description of rib

Figure 2.3-5 Lenticular Rib Geometry

15

Mesh attachment is provided for by the addition of hollow eyelets installed near the parabolic edge of the rib. The purpose of these eyelets is to protect the sewing thread from the chafing that would result from bare graphite epoxy holes.

The mesh chosen for the MSDA reflector (illustrated in Figure 2.3-6) is a Dacron fiber woven into a leno weave marquisette and manufactured by Travis Mills Corporation; its major characteristics are listed in Table II-4. The Dacron mesh is copper-coated and then has an outer protective silicone coating. The designation for this mesh is T635/Cu/6-1104. It is the same mesh used on the ATS-6 reflector, and its properties are fully reported in Document No. 5177259 titled "ATS F&G Parabolic Reflector Subsystem Antenna Mesh" dated January 15, 1974. LMSC has extensive experience with the T635 mesh and its use as a reflector material. Electrical performance of the mesh is discussed further in Section 3.2.2.

2.4 FEED MAST DESCRIPTION

The demand for large space platforms and antenna systems has identified the need for extremely long, stiff deployable booms. This need has prompted Lockheed Missiles and Space Company to develop a deployable space mast structure capable of repeatable precision deployments in the space environment without external aids. The structure, shown in Figure 2.4-1, is made up of longitudinal columns and cross braces which are doubly tapered graphite-epoxy tubes for maximum strength/weight ratio and stowing efficiency. The longitudinal members are hinged at the midpoint with a simple virtual hinge mechanism to provide a compact folding scheme. Small diameter tension rods serve as diagonal members. Pretensioning of these diagonals eliminates clearance in the longeron pivot bearings which ensures structural continuity and provides the majority of torsional stiffness. These features integrate into a truss system that exhibits a stiffness per unit length ratio and a stowage efficiency unsurpassed by any currently available design approaches.
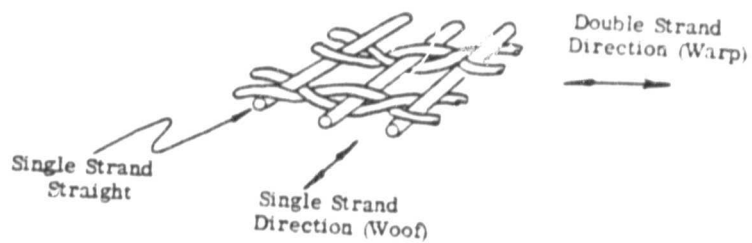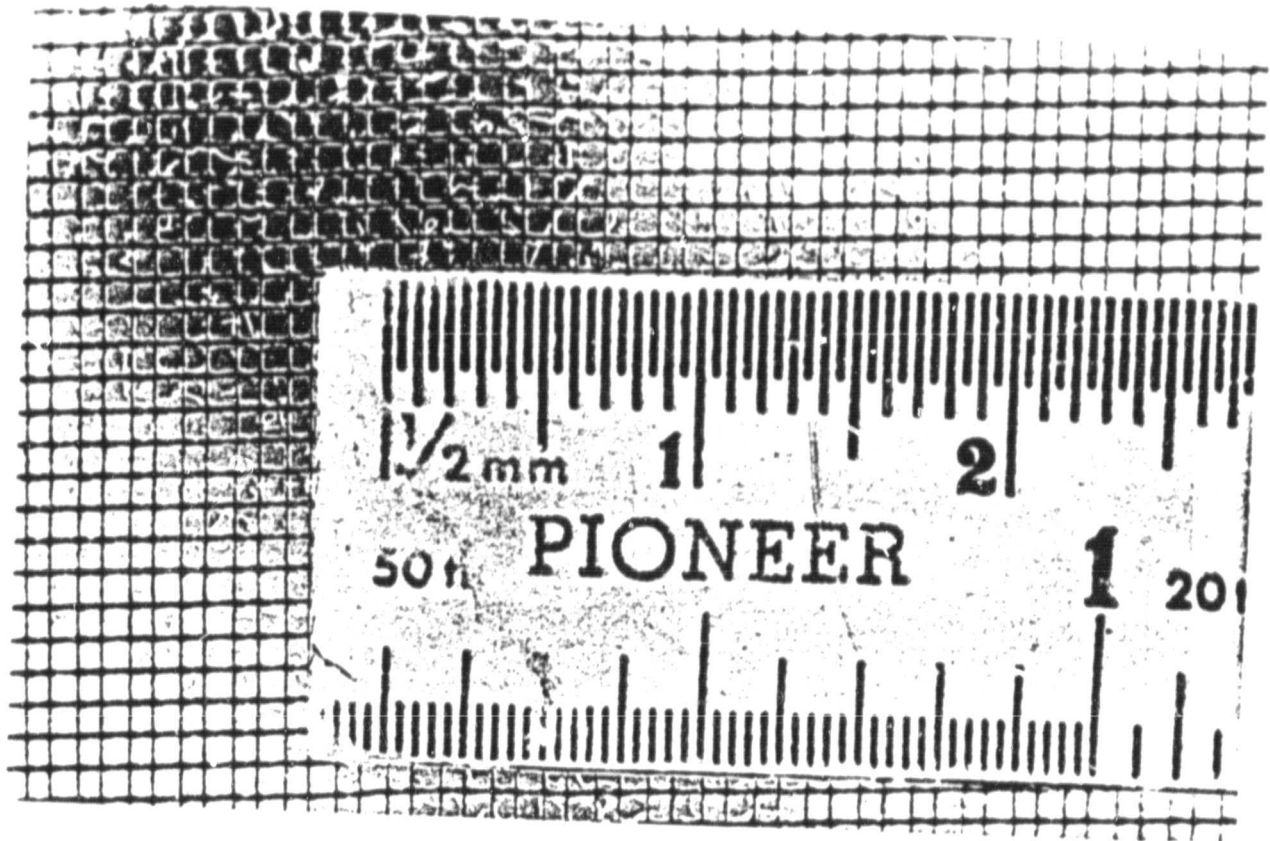
Figure 2.3-6 Woven Dacron Reflector Mesh

LOCKHEED MISSILES & SPACE COMPANY, INC.

TABLE II-4

DACRON MESH SUBSTRATE

1. SOURCE   - Style 635, Travis Mills Corporation, New York, NY

2. TYPE   - Leno weave marquisette

3. YARN   - High tenacity dacron, 70 denier, 14 filaments

Longitudinal direction: Twisted pairs of warp yarns, .98 pr/mm

Transverse direction: Single fill yarns, 1.18/mm

Melamine sizing

Filament diameter: 0.23 mm

Yarn cross section: 4.067×10^{-5} mm^2

LOCKHEED MISSILES & SPACE COMPANY. INC.
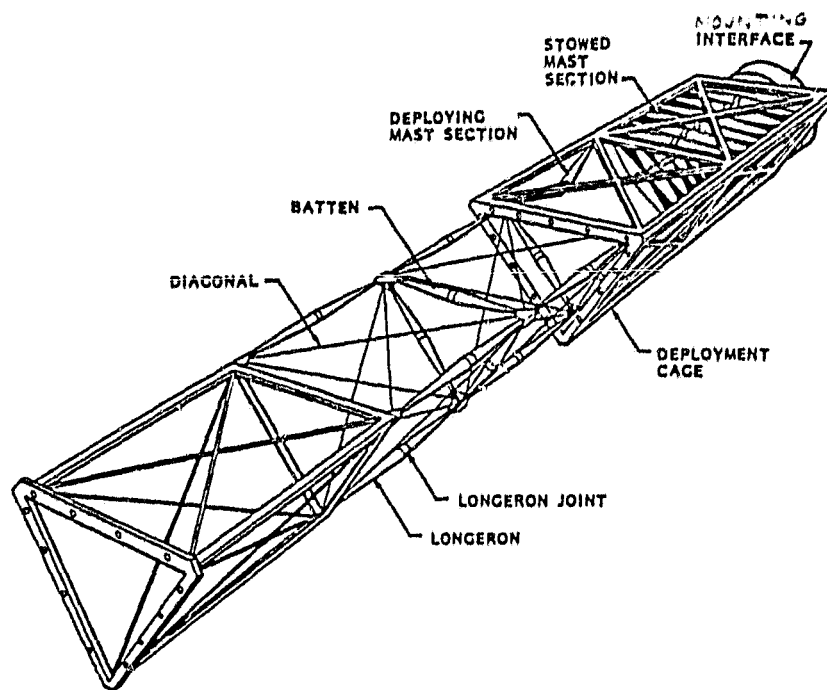
Figure 2.4-1 Feed Mast Components

19

The mast is deployed and retracted sequentially bay by bay, the extension sequence is illustrated in Figure 2.4-2. The stowed mast is held in deployment cages which are functionally divided into two compartments, one for handling the stowed mast and one for extending the bays. The stowed mast is slowly raised toward the forming compartment; the mechanism in the forming compartment lifts a single batten assembly and extends the longerons and diagonals of one bay until the bay is fully formed. This process is repeated until the complete mast is fully formed. These steps are reversed to retract the mast. A simplified schematic of the device is pictured in Figure 2.4-3 which illustrates the high/low speed drive arrangement and the function of the gear boxes, driver and belts. A significant design feature of the deployment mechanism is that during deployment loads are transmitted through the deployed mast sections into the upper deployment cage and around the deploying sections. This feature assures a predictable structural stiffness throughout the entire deployment operation.

The mast physical properties are detailed in Table II-5. The bay size was selected to provide the greatest cross section compatible with the STS Orbiter Cargo Bay stowage requirement. The other key design parameters are chosen to provide the highest overall deployed vibration frequency compatible with the known kinematic and system stowage constraints.

The mast design has been carried to construction of individual scale longeron elements to verify the longeron fold joint kinematics and beam strength.

The reflector support mast is of the same design as the feed support mast except that it contains one unique bay which forms the "knee joint" near the middle of the structure.
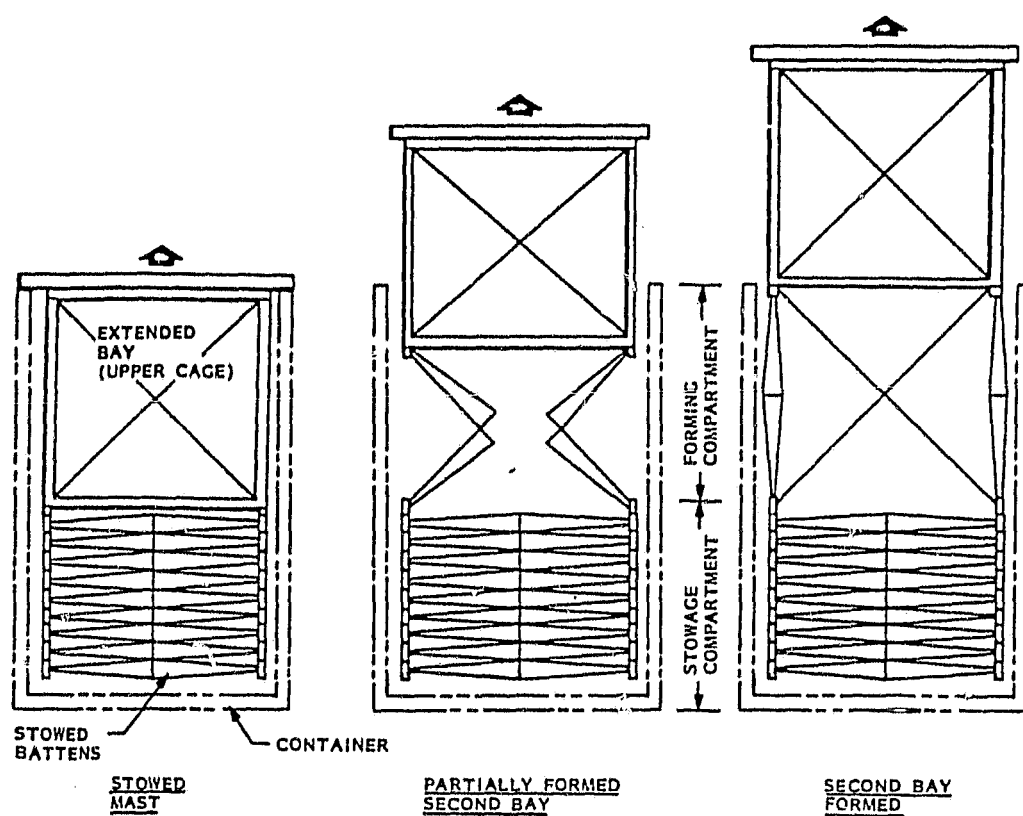
Figure 2.4-2 Mast Structure Deployment Schematic

21
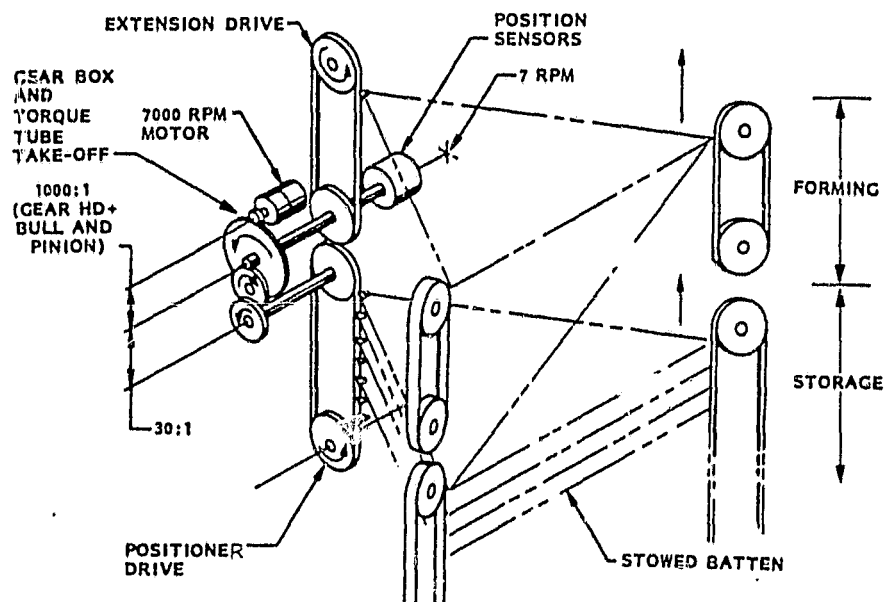
Figure 2.4-3 Mast Extension Drive Schematic

22

This bay is formed by deploying a single longeron and pivoting the mast about an axis passing through the other two corners of that bay, thus forming a single tetrahedular bay embedded within the normal mast. This arrangement allows the same mast deployment apparatus to deploy this bay.

2.5 COUNTERWEIGHT DESCRIPTION

The offset antenna requires a set of counterweights to dynamically balance the rotating system. Figures 2.5-1 and 2.5-2 shows families of mass/ offset curves which satisfy the dynamic balance requirement for the two possible spin axes giving a 35° scanning angle. These curves were obtained from a parametric computer optimizing routine assuming lumped masses of 270 kg at the feed and 185 kg at the reflector. Two masses of the sizes listed on the curves located at the points shown achieve dynamic balance for the reflector assembly. As can be seen from these figures arranging the spin axis as shown in Figure 2.5-1 is less sensitive to counterweight positioning tolerances. That spin orientation was there- fore selected for the design. The masses are supported from the antenna system by means of extendible booms of the stem real type (see Figure 2.5-3). This design has been selected because of its simplicity, low stowed volume and extensive successful development and flight experience. Documentation of the bistem boom configuration and design parameter infor- mation can be found in the proceedings of the 2nd Aerospace Mechanisms Symposium of May 4 - 5, 1967, NASA Technical Memorandum TM 33-355.

Table II-5 MAST PROPERTIES

PARAMETER		FEED MAST		REFLECTOR MAST
Length		13.3 m		21.3 m
Weight – Longerons	10.3 Kg		16.5 Kg	
Battens	10.6 Kg	30.9 Kg	17.0 Kg	49.5 Kg
Diagonals	10.0 Kg		16.0 Kg	
Bay Width		2.66 m		2.66 m
Bay Aspect Ratio		1:1		1:1
Number of Bays		5		8
Longeron Diameter – Maximum		10.0 cm		10.0 cm
Minimum		2.54 cm		2.54 cm
Longeron Thickness		.79 mm		.79 mm
Material		Graphite Epoxy Thermal 50		Graphite Epoxy Thermal 50
Stiffness (Bending)		$289 \times 10^3 \ \frac{N}{M}$		$113 \times 10^3 \ \frac{N}{M}$
(Torsion)		$294 \times 10^3 \ \frac{N\text{-}M}{rad}$		$115 \times 10^3 \ \frac{N\text{-}M}{rad}$
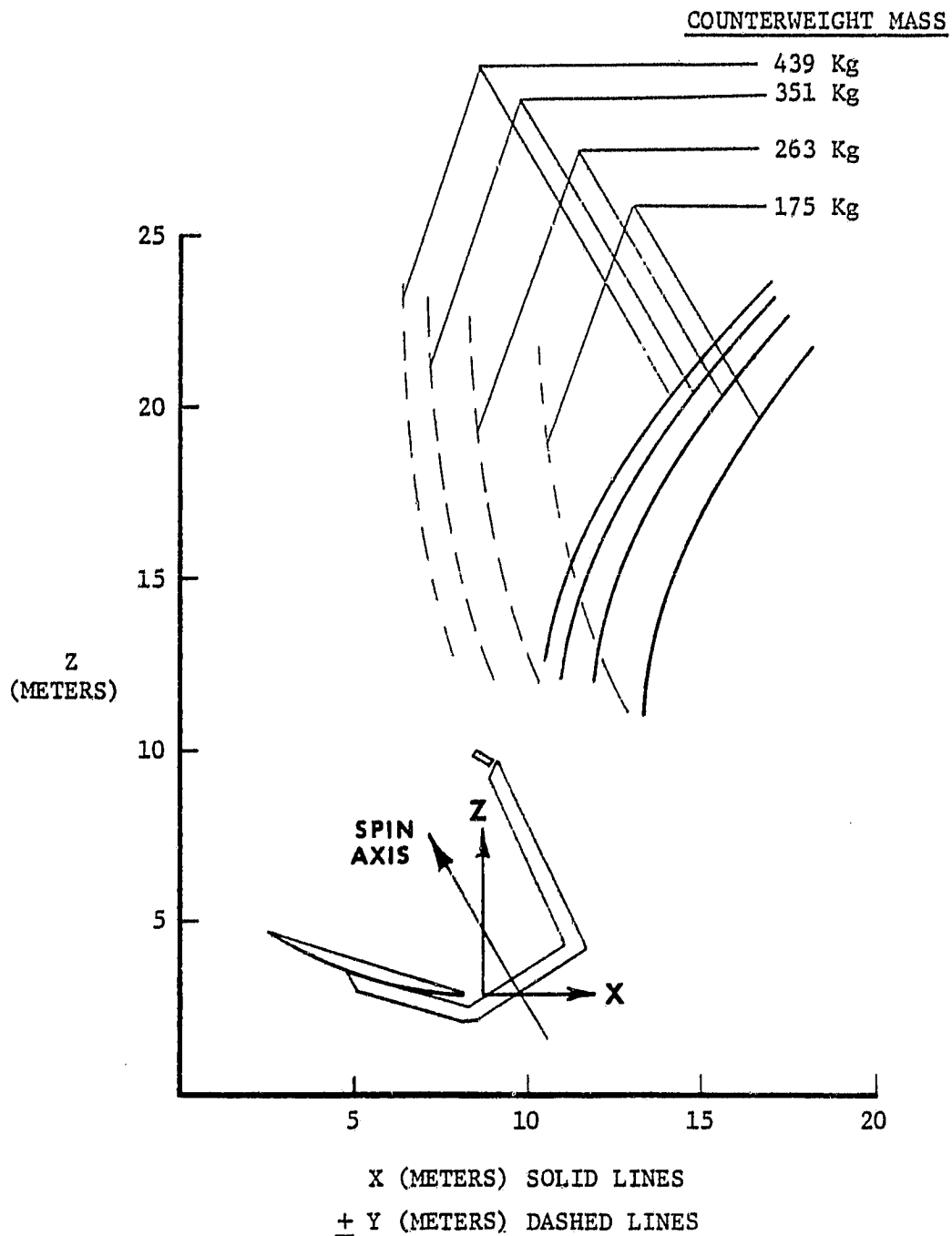
Figure 2.5-1 Counterweight Positions

25
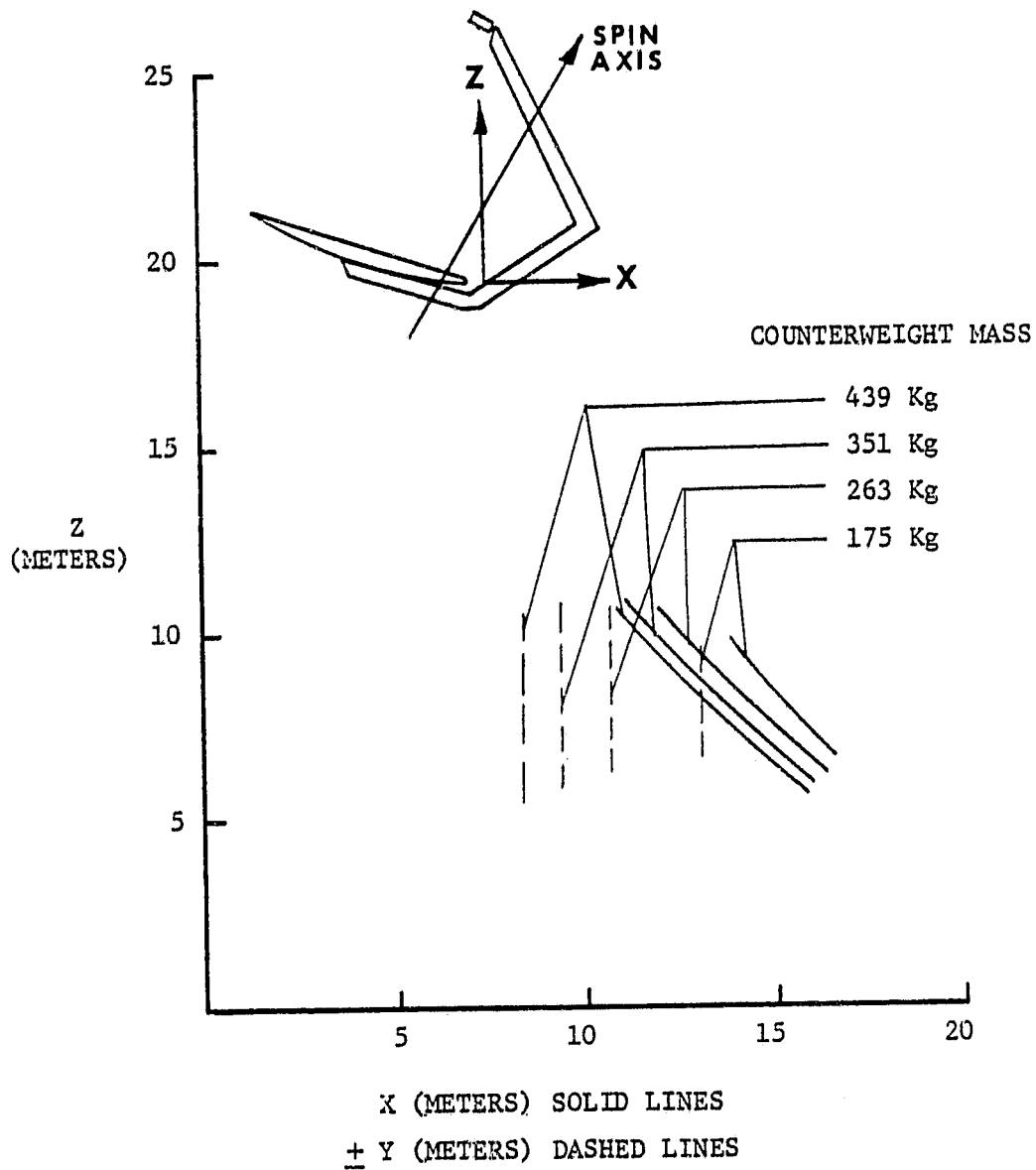
Figure 2.5-2 Counterweight Positions

26
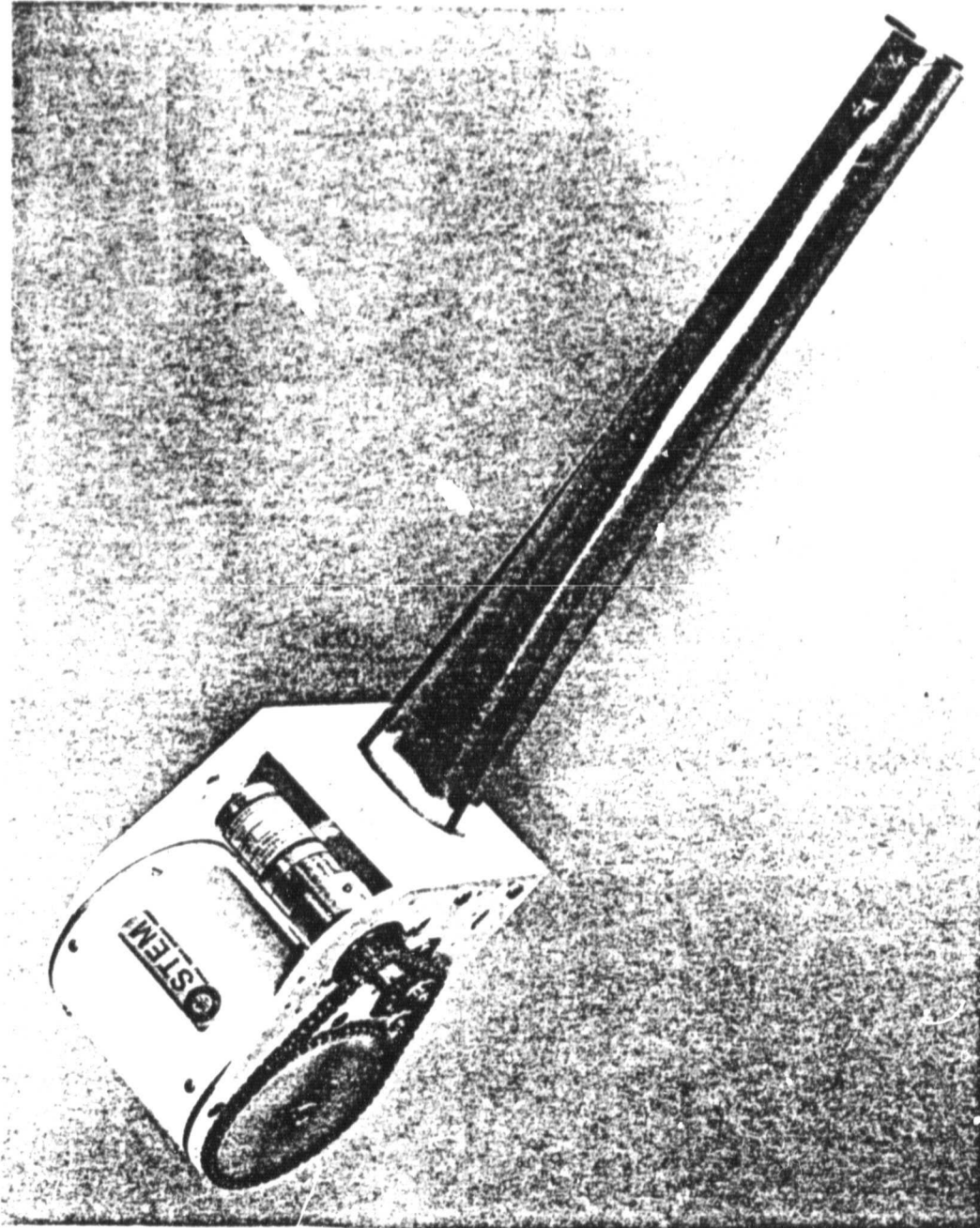
Figure 2.5-3 Extendible Reel (Bi-Stem) Boom

27

3.0 MAIN BEAM EFFICIENCY EVALUATION

The 15 m antenna system was analyzed to identify the individual error
components which effect the overall main beam efficiency. These analyses
which addressed electrical and mechanical error contributors are detailed
in this section. In summary the maximum achievable main beam efficiency
which can be expected for the off axis beam at frequencies of 5.1 GHz and
lower is 0.83. This limitation results from the achievable performance
of a simple feed aperture for the scanned beam case. The result should
not be considered conservative since the feed model was ideal in that the
pattern was perfectly axisymmetric which is difficult to achieve in hard-
ware. The 11 GHz case is aided by the under illuminated aperture and the
longer apparent focal length to yield a scanned beam efficiency of 0.89.
This case illustrates the benefits which could be achieved at the low fre-
quencies by employing multiple apertures for beam forming or extremely
long focal lengths. The individual errors and overall performance devel-
oped for the antenna are displayed in Figure 3.0-1. These data are refer-
enced to the appropriate sections which contain details of the analyses
performed.

3.1 METHOD OF RF ANALYSIS

The secondary far field patterns of a parabolic reflector were obtained
by using the efficient, versatile Fourier Bessel method just developed
by Dr. Charles C. Hung of the RF/Antenna Systems, LMSC. The secondary
field of an arbitrary reflector can be expressed in terms of physical-
optics integral of the current on the reflector. There exist many tech-
niques to evaluate, or compute, this physical optics integral. For scan
cases all these previously developed techniques become essentially imprac-
tical from cost and computer time considerations. The Fourier Bessel

ERROR	REF. SECTION	5.1 GHz		11 GHz	
		ON-AXIS	SCANNED	ON-AXIS	SCANNED
ILLUMINATION, CROSS POLARIZATION, SPILLOVER	3.2	9.9172	0.9172	0.9237	0.9237
SCAN	3.2	-	0.9378	-	0.9944
THERMAL*	3.3.1	0.9999	0.9999	0.9999	0.9999
APPROXIMATION	3.3.3	0.9708	0.9708	0.9704	0.9704
MANUFACTURING*	3.3.4	0.9991	0.9991	0.9987	0.9987
ROTATION*	3.3.5	0.9959	0.9959	0.9975	0.9975
MESH	3.3.2	0.9999	0.9999	0.9999	0.9999
TOTAL		0.8858	0.8307	0.8928	0.8878

*Based on Aperture Efficiency Calculation

Figure 3.0-1 15 m Antenna Main Beam Efficiency

29

method is very versatile and can be employed for any reflector shape such as a spherical reflector, reflectors with surface errors and those reflectors with projected aperture shapes that deviate from the familiar circular geometry, as for instance, a polygonal-shaped aperture.

In the Fourier Bessel method, the integrand of the physical optics integral for a reflector is first expanded in terms of the well known sinusoidal functions and the integration is carried out analytically with the aid of a shape function. This expansion of the integrand into sinusoidal functions does not depend on the reflector geometry and is accomplished via the well established Fast Fourier Transform (FFT) algorithm. The far field is then expressed in terms of a summation of a series of Airy functions for a circular projected reflector aperture and a series of tangent and exponential functions for a polygonal shaped projected reflector aperture. The convergence of this resultant series is very good even for wide angle scan cases and hence can be evaluated using very little computer time. The details of this Fourier-Bessel method to compute the secondary far field pattern will be published soon.

For scan beam cases, one important design information is the location of feed elements. This information can be obtained by using the focal region distribution of the reflector when it is operating in receiving mode and is illuminated by a plane wave incident from the intended direction of scan. By reciprocity theorem, the focal region distribution can be obtained by repeatedly computing the radiated far field of the same reflector for different feed positions in its focal region. With the efficient Fourier Bessel method, the focal region distribution can be generated without incurring high computer cost to provide the correct feed element location for the given scan angle.

The main beam efficiency can be computed by integrating the main beam pattern and comparing to the total energy radiated. Again, with the efficient Fourier Bessel method of computing the far field pattern, it

is now possible to perform the pattern integration on the computer with
a very reasonable computer time.

3.2 RF ANALYSIS

In order to determine the total main beam efficiency of the perfect off-
set antenna the far field patterns of the offset parabolic reflector
were obtained. The feed element used in the analysis was a linearly
polarized circular aperture with uniform distribution across the aper-
ture, hence the feed pattern is an Airy function. The radius of this
circular aperture was chosen to maximize the 5.1 GHz main beam effici-
ency of the on axis case for an F/D = 1.0 offset geometry. In this case
the F/D represents the ratio of the actual system focal length to the
projected circular aperture diameter perpendicular to the axis of the
main beam. The main beam efficiency maximized at 91.72% with a feed
aperture radius of 76.96 mm (3.03 in.). This maximum main beam effic-
iency feed diameter produces -10 dB power edge directed illumination.
The resulting surface current distribution projected and circular aper-
ture plane is shown in Figure 3.2-1 and the far field pattern in Figure
3.2-2. The calculated efficiency was obtained by pattern integration
between the first nulls referenced to the total energy radiated by the
feed. As a result this efficiency includes the effects of (1) aperture
illumination, (2) cross polarization, and (3) spillover inherent in the
calculation for the offset antenna.

After the on-axis case efficiency was optimized the case with the beam
scanned 1.627 degrees or 5.5 beam widths off axis was calculated. For
this case the direction of scan was from the focal point radially toward
the outer edge of the reflector in the direction of the offset. The
results are shown in Figure 3.2-3 with a calculated efficiency of 80.18%.
This result indicated substantial scan impacts which are incompatible
with the desired 90% efficiency requirement. The system F/D was then
varied to evaluate the ability to reduce the scan effects to an

31

D = 590.55 F/D = 1.0

H = 374.02

FREQ = 5.1 GHZ

NO SCAN

SINGLE FEED AT

0.0,0.0,0.0,0

3.03 INCH FEED
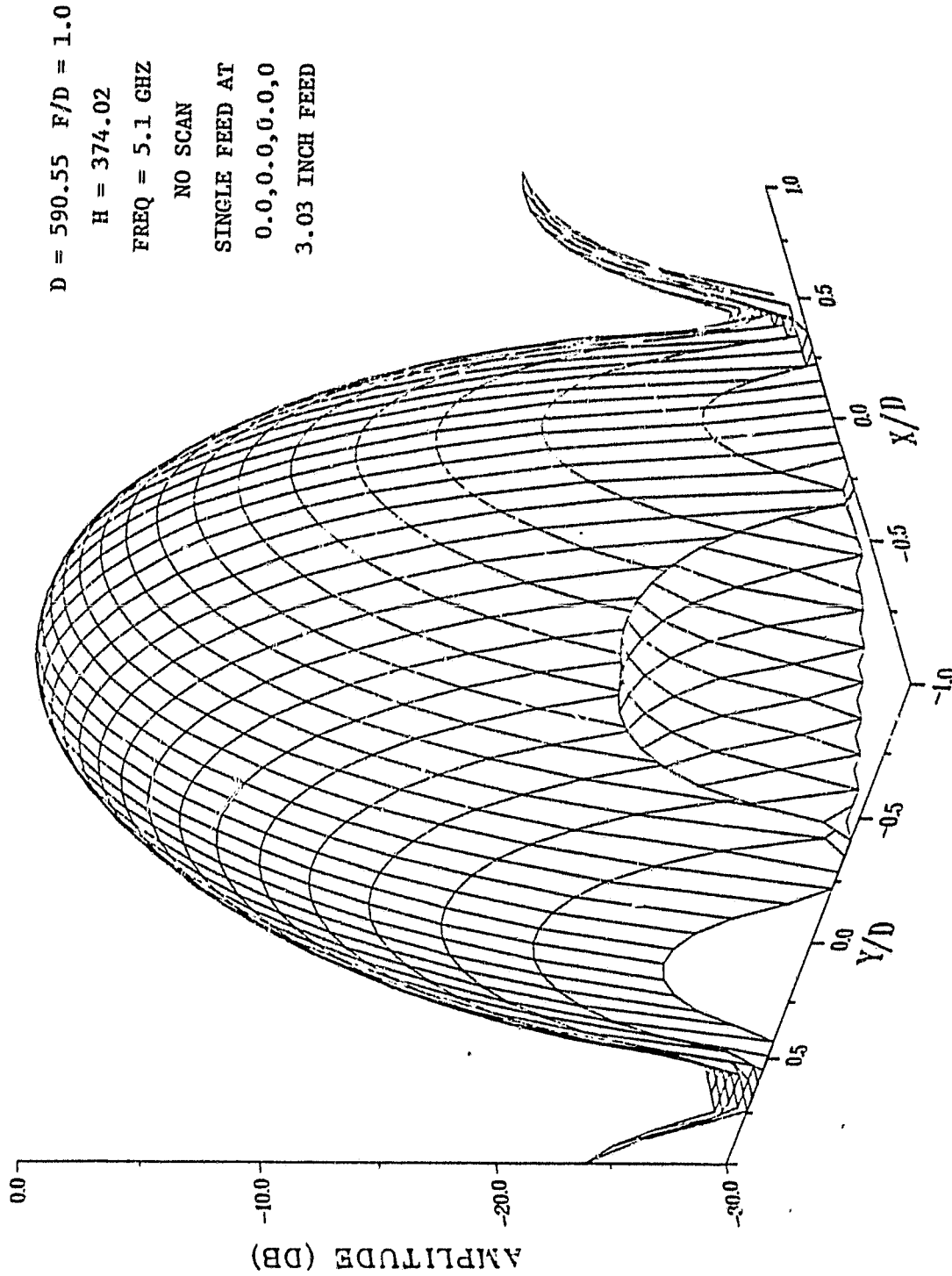
Figure 3.2-1 Equivalent Surface Current, On-Axis, 5.1 GHz

32

FAR FIELD PATTERN AT V=0.0

FAR FIELD PATTERN AT U=0.0

OFFSET PARABOLIC
REFLECTOR

D = 590.55   F/D = 1.0

H = 374.02

FREQ = 5.1 GHZ

FEED RADIUS = 3.03

FEED AT

(0.0,0.0,0.0)

MAIN BEAM EFFICIENCY =

0.917

Figure 3.2-2 On-Axis Pattern, 5.1 GHz, F/D = 1.0

33

FAR FIELD PATTERN AT V=SIN(1.627)

MAIN POL
CROSS POL

GAIN (DB)

U

FAR FIELD PATTERN AT U=0.0

MAIN POL
CROSS POL

GAIN (DB)

V

OFFSET PARABOLIC
REFLECTOR
D = 590.55 F/D = 1.0
H = 374.02
FREQ = 5.1 GHZ
FEED RADIUS = 3.03
FEED AT
(0.0,-15,00,-11.50)

MAIN BEAM EFFICIENCY =
0.808
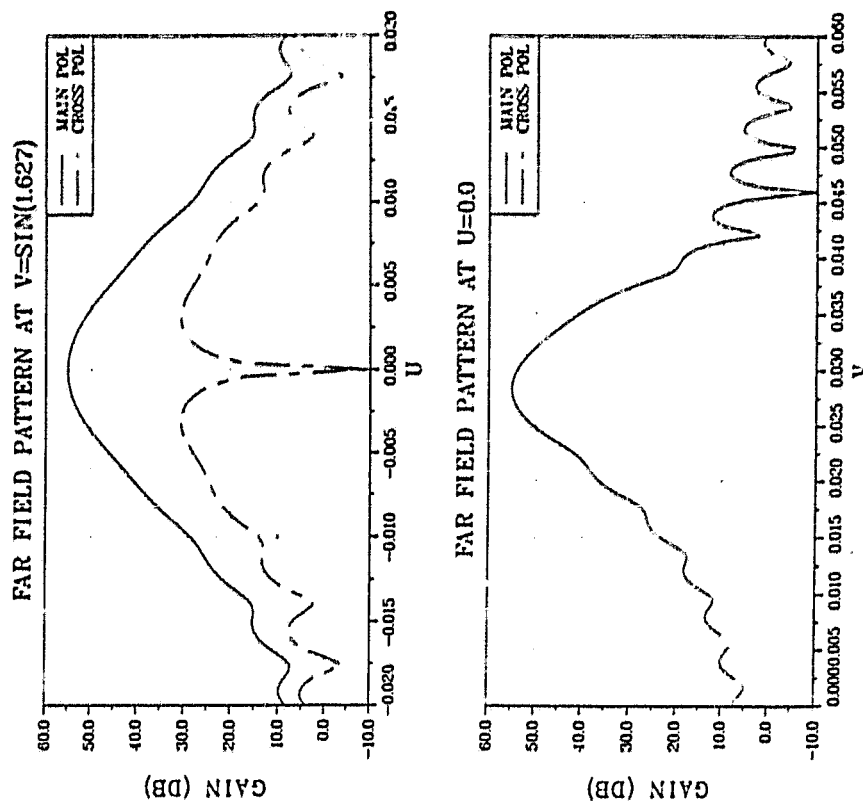
Figure 3.2-3   Scan Beam Pattern, 5.1 GHz, F/D = 1.0

34

LOCKHEED MISSILES & SPACE COMPANY. INC.

acceptable level. Since the problem was isolated to the effects of scan
the feed was not re-optimized for the study of F/D efficiency variation.
This results in the calculated efficiencies use being restricted to rel-
ative evaluation.

Figures 3.2-4, 3.2-5, 3.2-6 and 3.2-7 present the resulting far field
patterns for the on axis and scanned cases for F/D = 1.25 and 1.5 respec-
tively. These results indicate that the efficiency effect due to scan
for the F/D = 1.25 case is 0.912 and the F/D = 1.5 is 0.9378. The on
axis efficiencies for both cases can be increased to the 0.9172 calcu-
lated for the F/D = 1.0 case with re-optimized feed diameter so the
achievable total efficiency for the scanned F/D = 1.25 system is 0.8365
and for the F/D = 1.5, 0.8553. Some additional improvement in these
total efficiencies would result from re-calibration since the cross
polarization effects are also reduced by the longer focal lengths and
these reductions are not included without rigorous re-calculation.

At this point selection of an F/D = 1.5 is indicated as the necessary
geometry to achieve a near 90% efficiency requirement. With this sel-
ection of F/D the under illuminated case was investigated. The feed
function was adjusted by varying the feed radius to achieve an 0.35
degree beamwidth at 11.0 GHz. This was obtained with a radius of 81.28
mm (3.20 inches). The resulting aperture surface currents are presented
in Figure 3.2-8. Both the on axis and 1.575 degrees scanned far field
patterns were then calculated. These results are presented in Figures
3.2-9 and 3.2-10. The calculated main beam efficiencies are 0.9237 for
the on axis beam and 0.9185 for the scanned beam.

The results of the pattern analysis thus indicate in summary that an F/D
= 1.5 system is required to reduce the effects of scan losses on effic-
iency to acceptable levels. The calculations indicate a worst case main
beam efficiency of 0.8553 at 5.3 GHz for the beam scanned 1.627 degrees
(5.5 beamwidths) off axis and 0.9185 at 11 GHz for the beam scanned

35

FAR FIELD PATTERN AT V=0.0

MAIN POL
CROSS POL

FAR FIELD PATTERN AT U=0.0

MAIN POL
CROSS POL

OFFSET PARABOLIC
REFLECTOR

D = 590.55   F/D = 1.25

H = 374.02

FEED RADIUS = 3.03

FEED AT

(0.0, 0.0, 0.0)

MAIN BEAM EFFICIENCY =

0.878

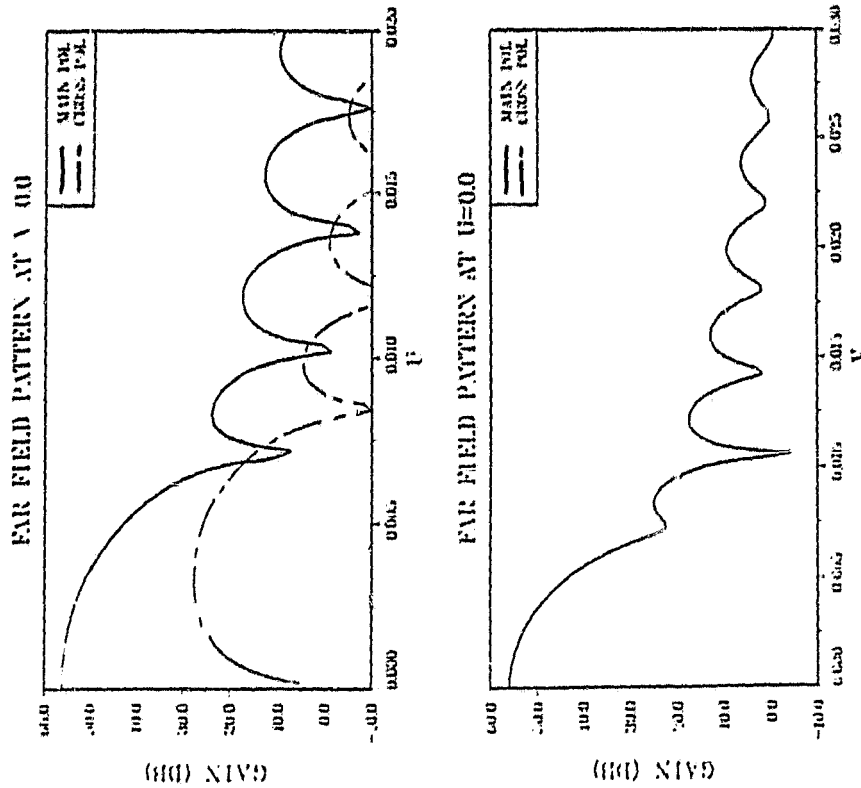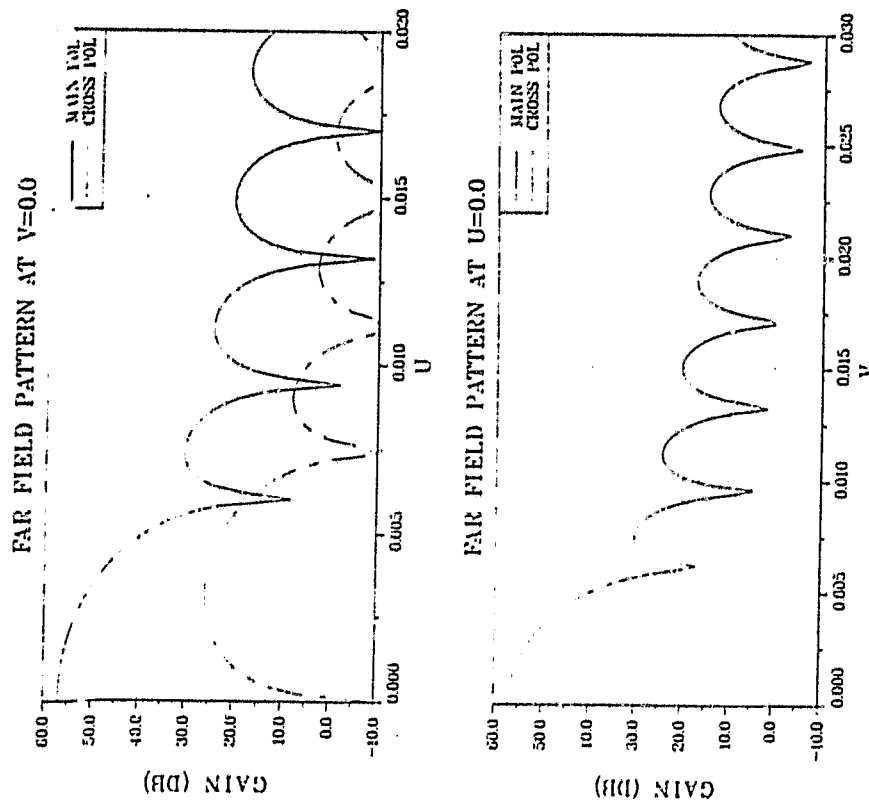Figure 3.2-4   On-Axis Pattern, 5.1 GHz, F/D = 1.25

LOCKHEED MISSILES & SPACE COMPANY, INC.

FAR FIELD PATTERN AT V=SIN(1.627)

FAR FIELD PATTERN AT U=0.0

OFFSET PARABOLIC
REFLECTOR

D = 590.55 F/D = 1.25

H = 374.02

FREQ = 5.1 GHZ

FEED RADIUS = 3.03

FEED AT

(0.0,-20.00,-11.00)

MAIN BEAM EFFICIENCY =

0.8007
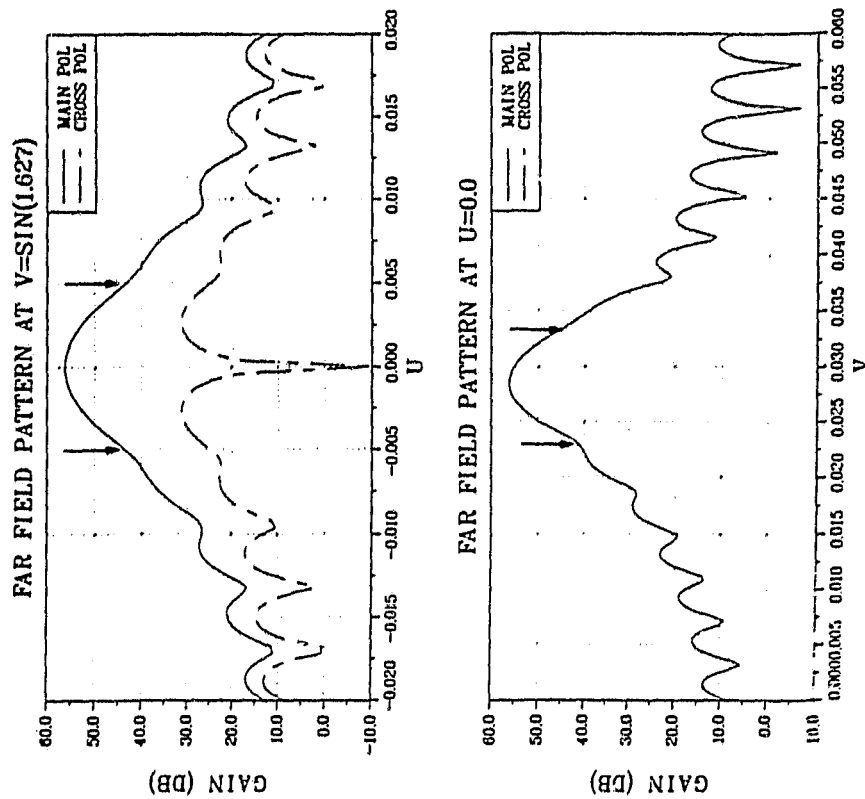
Figure 3.2-5 Scan Beam Pattern, 5.1 GHz, F/D = 1.25

37

FAR FIELD PATTERN AT V=0.0

FAR FIELD PATTERN AT U=0.0

OFFSET PARABOLIC
REFLECTOR

D = 590.55 F/D = 1.50

H = 374.02

FREQ = 5.1 GHZ

FEED RADIUS = 3.03

FEED AT

(0.0,0.0,0.0)

MAIN BEAM EFFICIENCY =

0.8531
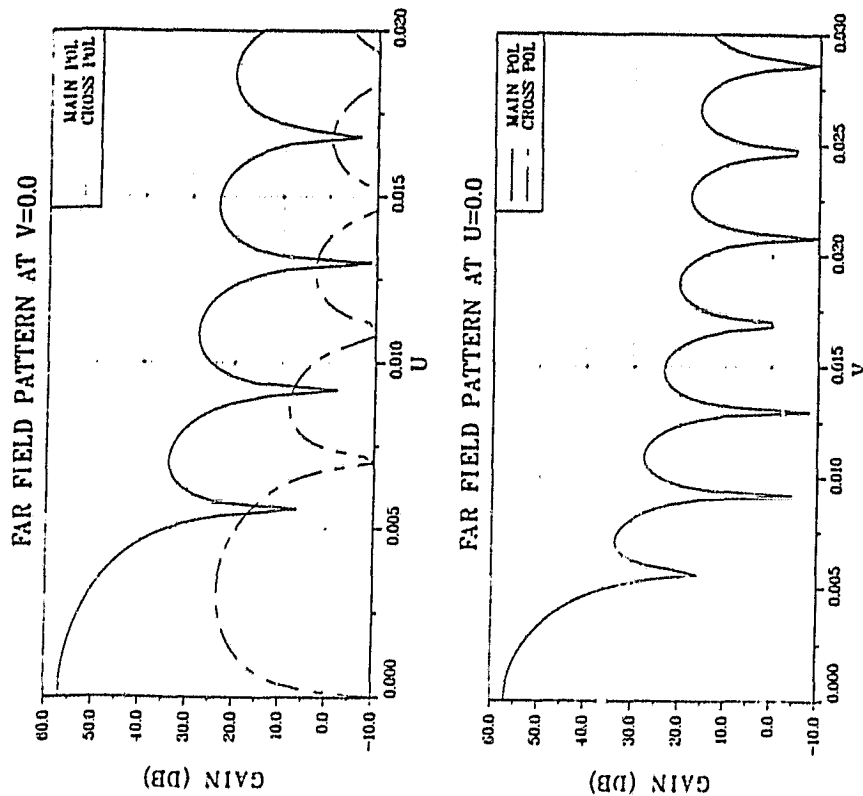
Figure 3.2-6 On-Axis Pattern, 5.1 GHz, F/D = 1.5

38

OFFSET PARABOLIC
REFLECTOR

D = 590.55 F/D = 1.50

H = 374.02

FREQ = 5.1 GHZ

FEED RADIUS = 3.03

FEED AT

(0.0,-24.00,-11.50)

MAIN BEAM EFFICIENCY =

0.8000
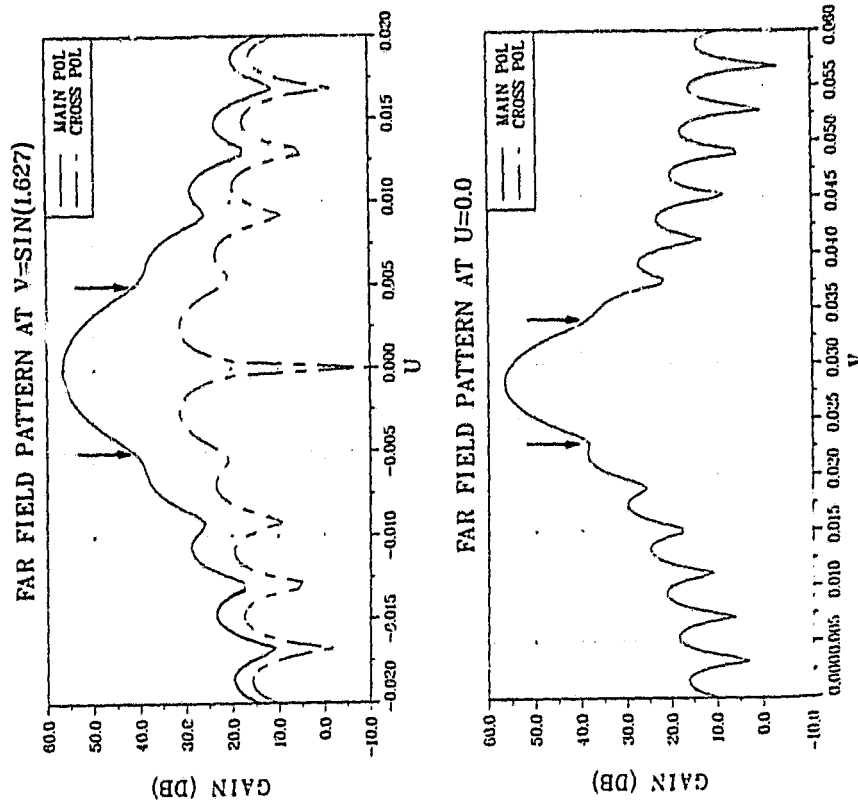
Figure 3.2-7 Scan Beam Pattern, 5.1 GHz, F/D = 1.5

LOCKHEED MISSILES & SPACE COMPANY, INC.

OFFSET REFLECTOR

D = 590.55 F/D = 1.50 H = 374.02

H = 374.02

FREQ = 11.0 GHZ

NO SCAN

SINGLE FEED AT

0.0,0.0,0.0,0

3.20 INCH
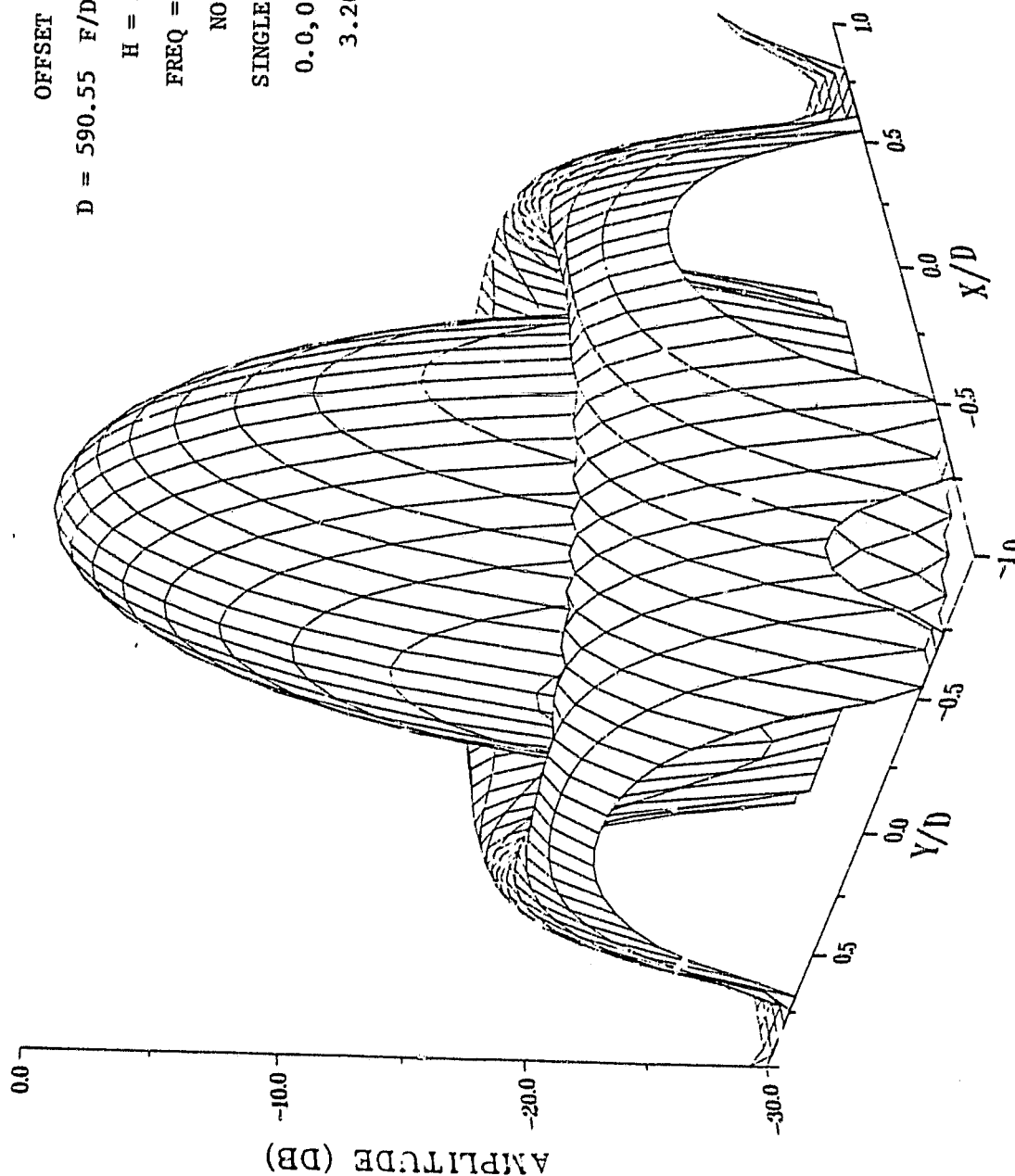
Figure 3.2-8 Equivalent Surface Current, On-Axis, 11 GHz

AMPLITUDE (DB)

40

FAR FIELD PATTERN AT V=0.0

FAR FIELD PATTERN AT U=0.0

OFFSET PARABOLIC
REFLECTOR

D = 590.55 F/D = 1.50

H = 374.02

FREQ = 11.0 GHZ

RADIUS = 3.20

FEED AT

(0.0,0.0,0.0)

MAIN BEAM EFFICIENCY =

0.9237
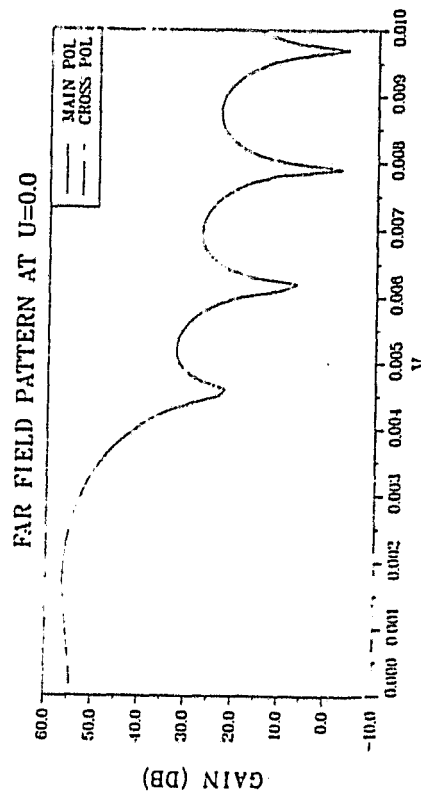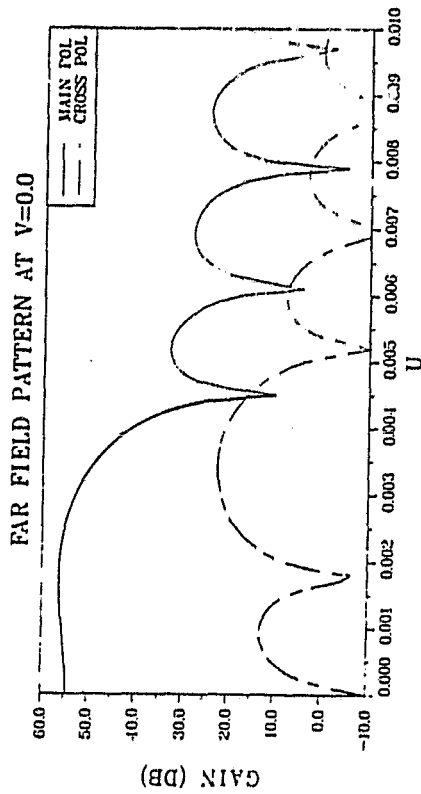
Figure 3.2-9. On-Axis Pattern, 11 GHz, F/D = 1.5

41

FAR FIELD PATTERN AT V=SIN(1.575)

FAR FIELD PATTERN AT U=0.0

OFFSET PARABOLIC
REFLECTOR

D = 590.55 F/D = 1.50

H = 374.02

FREQ = 11.0 GHZ

SINGLE UNIFORM

FEED AT

(0.0,-23.50,-10.50)

MAIN BEAM EFFICIENCY =

0.9185
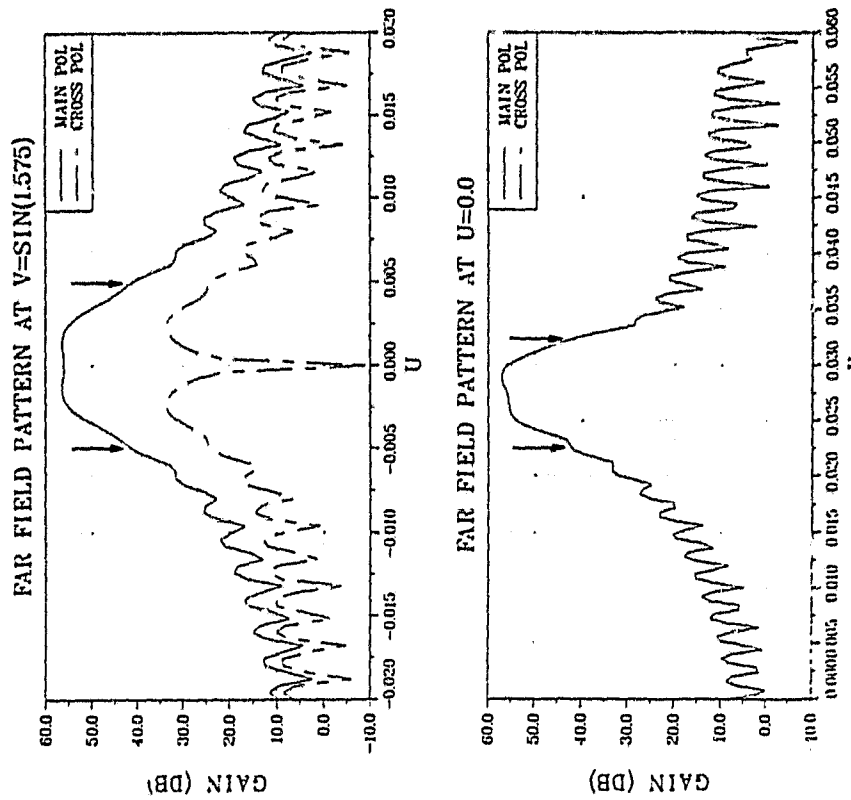
Figure 3.2-10   Scan Beam Pattern, 11 GHz, F/D = 1.5

42

1.575 degrees (4.5 beamwidths) off axis. These efficiencies include the effects of aperture illumination, cross polarization, spillover and off axis scan.

3.3 MECHANICAL ANALYSIS

The results of the electrical analysis indicate that in order to achieve a 90% main beam efficiency at 11 GHz the allowable mechanical error budget is 0.9799. As previously indicated 90% efficiency at 5.1 GHz will not be achievable. This must include the effects of surface approximation, mesh, thermal distortion and mechanical scan of the antenna system. The following is a description of the analysis performed to bound the effects on efficiency of the individual mechanical errors.

3.3.1 Thermal Distortions

The orbit thermal analysis performed on the 15 meter diameter reflector investigated the quarter points of each of three orbits considered. These were sun angles of 0, 30 and 80 degrees with respect to the orbit plane. At each of the quarter points one spacecraft revolution was investigated. Temperature information was obtained for each of the four points during the spacecraft spin. These data were provided for the subsequent distortion analyses. In addition the average temperature was obtained for the orbit positions investigated by averaging the four point spin temperatures.

Based on previous study work on other programs it has been found that the rib depthwise temperature gradients, which have a primary effect on surface distortion, are proportional to the rib absolute temperature. Therefore, the colder the ribs run in orbit, the lower the temperature gradients and the lower the surface distortion. Since the antenna system was spinning and the solar arrays were assumed de-spun the effect

43

of the arrays is to cause the ribs, they repeatedly shadow during the
spinning, to run colder. Since this would produce smaller rib grad-
ients, it was felt that the arrays should be neglected thereby leading
to conservative predictions for performance.

A thermal model previously developed was used to obtain the heat rates
for each segment of the 15 meter reflector and was used to calculate
the thermal load conditions. Figures 3.3-1 and 3.3-2 present the nodal
breakdown used in the segmented approach to the determination of heat
rates. The temperature response for each sector was computed using the
model shown in Figure 3.3-2 with four other sector heat rates combined
with the sector of interest. The hub was modeled in detail as a typi-
cal hub structure. Figure 3.3-3 presents a cross section of a hub
thermal model. The hub consisting of upper and lower rings and a vert-
ical spacer is modeled in detail. The insulation around the hub is
modeled with inner and outer nodes connected with a radiation resistance
based upon an effective emittance factor. The outer surfaces of the
inter-rib curtains and insulation are Kapton aluminized on the backside
which results in an $\alpha = 0.4$ and $\epsilon = 0.6$. The inner surface of the cur-
tain is aluminum with an $\epsilon = 0.1$. The hub doors are anodized (DOW 17)
which results in an $\alpha = 0.78$ and $\epsilon = 0.7$. The rib surface optical prop-
erties were assumed to be those of a surface coated rib with $\alpha = 0.20$
and $\epsilon = 0.35$.

The thermal distortion analysis performed to obtain the distorted orbital
surface description was performed on a finite element computer program
SPAR. The program is based on the direct stiffness method of matrix
structural analysis. This program handles 17 types of finite structural
elements.

The reflector model employs quadrilateral constant thickness membrane
elements to model the mesh. In-plane displacements vary linearly along
the edges and within the element interior. Mesh stiffness properties

44
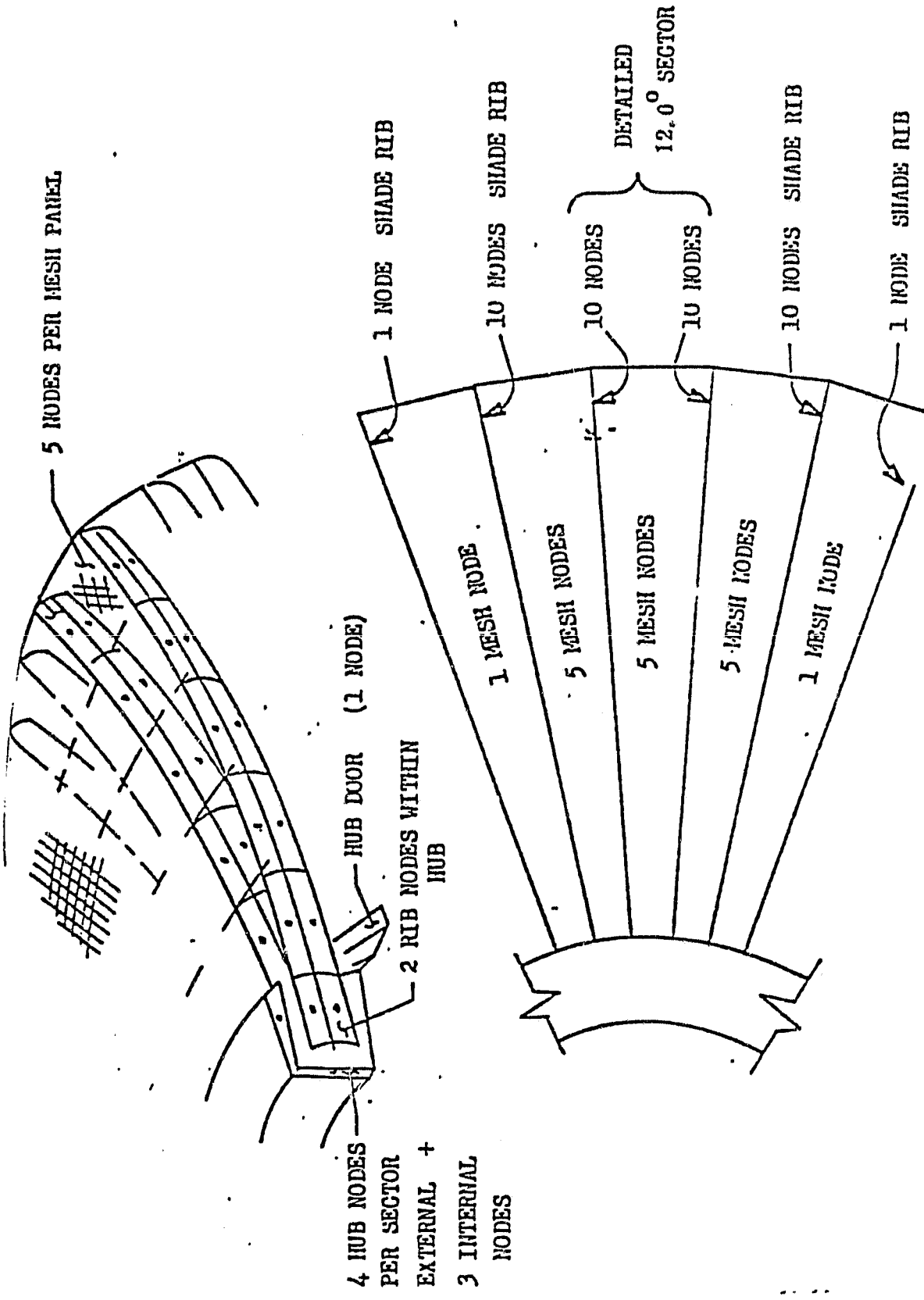
Figure 3.3-1 Detailed Thermal Analysis Approach Nodal Breakdown

45
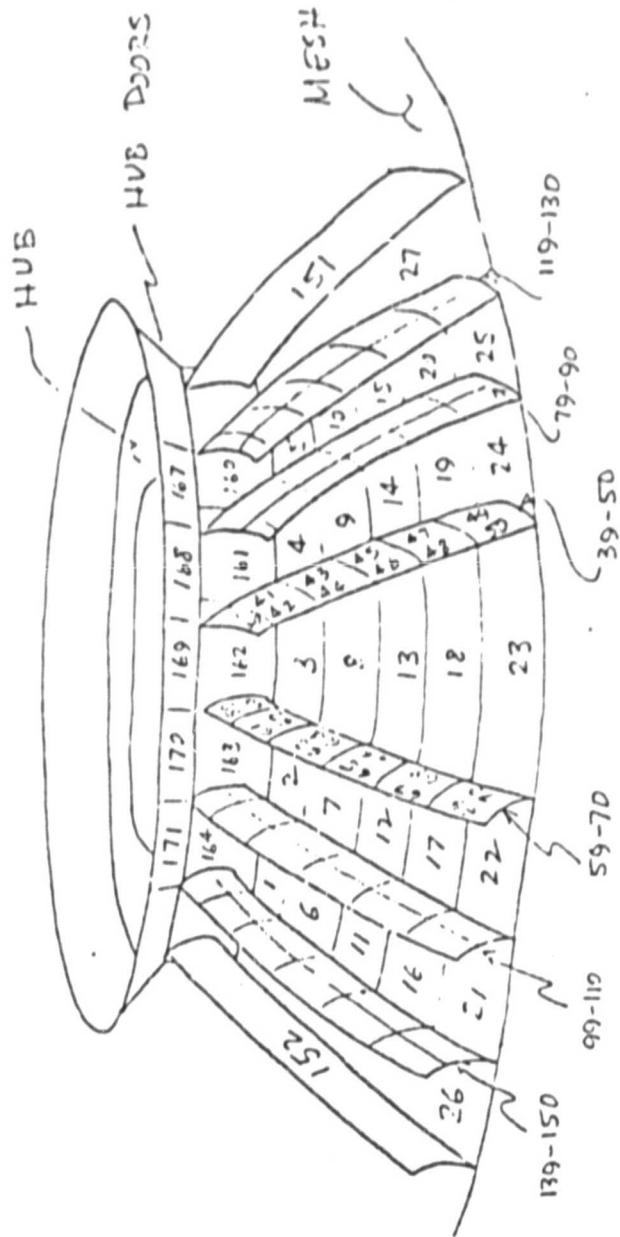
Figure 3.3-2 Nodal Breakdown

46
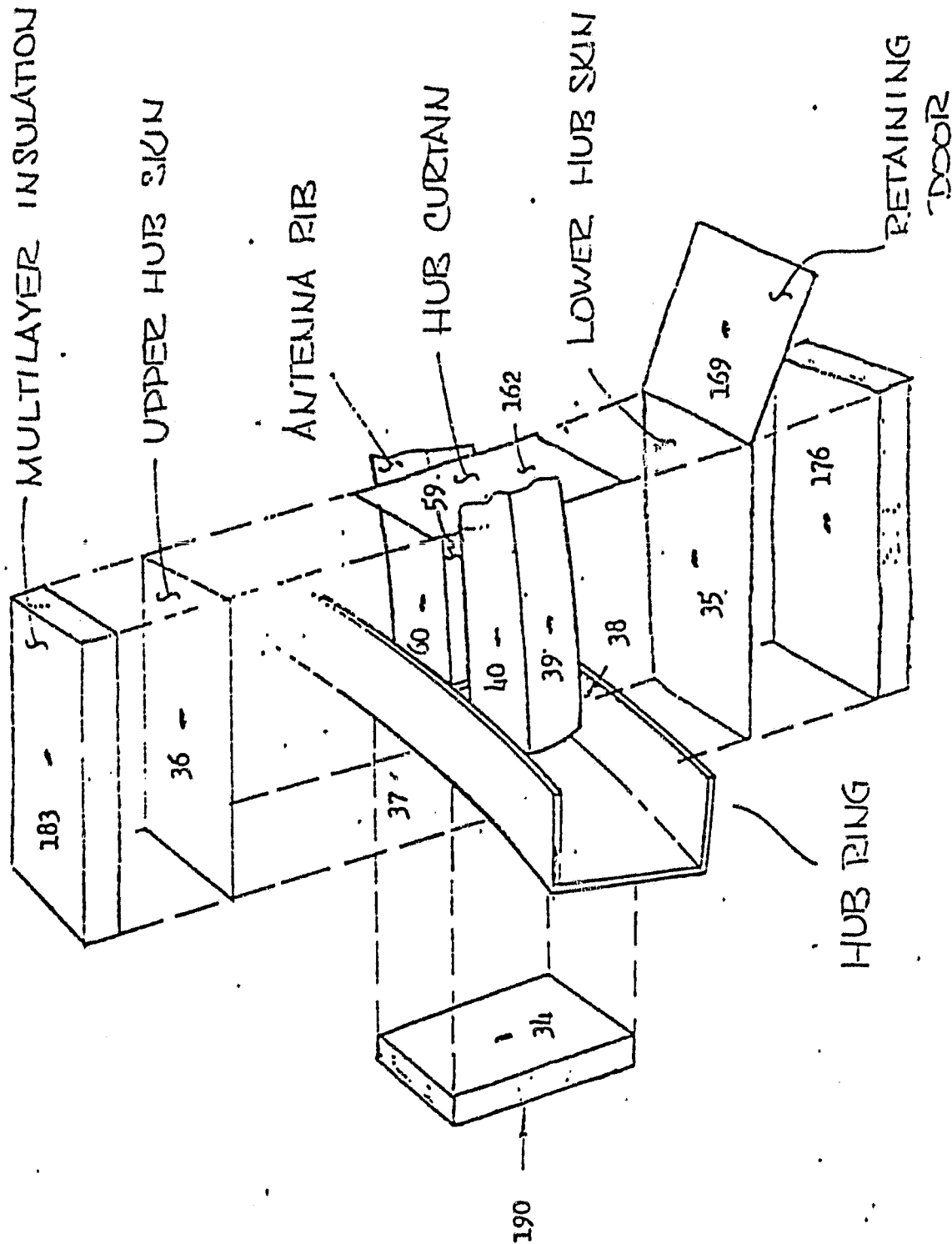
Figure 3.3-3 Hub Model

47

vary as a function of strain and temperature and the thermal coefficient
of expansion varies as a function of temperature.

The ribs are modeled as beam elements with primary and secondary bending
planes. The element line of mass and shear center are offset to allow
for the proper description of the rib properties.

The hub is modeled with plate, ring and beam elements depending on the
particular type of construction involved.

The loading conditions analyzed consist of the orbit thermal loads
applied to the mesh elements, rib elements and hub elements. These
loads are provided by absolute temperature changes as well as temper-
ature gradients and differences through the rib and hub elements.

The results of the thermal distortion analysis in terms of surface
weighted rms differences from the designed zero gravity wrap rib surface
are presented in Figure 3.3-4. In addition, the efficiency effects so
rigorous pattern calculation with the distorted surface was not pursued.

3.3.2 Mesh Effects

Previous testing of meshes at LMSC have resulted in identification of
mesh reflectivity efficiencies for both gold plated molybdenum wire and
copper plated dacron meshes. These tests indicate that gold plated wire
mesh can be knitted to provide a reflectivity efficiency of 0.972 at
11 GHz and 0.987 at 5.1 GHz. This measured efficiency includes both
the effects of energy transmitted through the material as well as the
energy absorbed by the material. The dacron mesh flown on the ATS-6
vehicle exhibits a reflectivity efficiency of 0.9992 at 11 GHz. Since
the highest possible efficiency is required and the thermal distortions,
based on the analysis presented in Section 3.3.1, are insignificant with
the dacron material, the dacron mesh should provide the best performance.

48

ORBIT	TIME	RMS FOR 5.1 GHz	η 5.1 GHz	RMS For 11 GHz	η 11 CHz
	0	$0.777 \times 10^{-3} \lambda$	0.999904	$0.746 \times 10^{-3} \lambda$	0.99991
$\beta = 0$	27	$0.605 \times 10^{-3} \lambda$	0.99994	$0.652 \times 10^{-3} \lambda$	0.99993
	54	$0.346 \times 10^{-3} \lambda$	0.99998	$0.373 \times 10^{-3} \lambda$	0.99998
	81	$0.605 \times 10^{-3} \lambda$	0.99994	$0.652 \times 10^{-3} \lambda$	0.99993
	0	$0.648 \times 10^{-3} \lambda$	0.99993	$0.652 \times 10^{-3} \lambda$	0.99993
$\beta = 30$	27	$0.605 \times 10^{-3} \lambda$	0.99994	$0.652 \times 10^{-3} \lambda$	0.99993
	54	$0.346 \times 10^{-3} \lambda$	0.99998	$0.373 \times 10^{-3} \lambda$	0.99998
	81	$0.605 \times 10^{-3} \lambda$	0.99994	$0.652 \times 10^{-3} \lambda$	0.99993
	0	$0.346 \times 10^{-3} \lambda$	0.99998	$0.373 \times 10^{-3} \lambda$	0.99998
$\beta = 80$	27	$0.605 \times 10^{-3} \lambda$	0.99994	$0.652 \times 10^{-3} \lambda$	0.99993
	54	$0.346 \times 10^{-3} \lambda$	0.99998	$0.373 \times 10^{-3} \lambda$	0.99998
	81	$0.605 \times 10^{-3} \lambda$	0.99994	$0.652 \times 10^{-3} \lambda$	0.99993

Figure 3.3-4   Effects of Orbit Thermal Distortion

49

For purposes of the efficiency calculation the 0.9999 will be used.
This neglects the slight benefit which would be gained by adjusting the
efficiency up to reflect the absorbed energy which will not contribute
to the antenna main beam efficiency degradation.

3.3.3 Surface Approximation Effects

The wrap rib surface approximation error has been well characterized.
Figure 3.3-5 presents patterns of the perfect surface and the parabolic
cylindrical gore approximation for the offset wrap rib at 5.1 GHz. The
resulting main beam efficiency change was calculated to be 0.9708. The
surface was also evaluated at 11 GHz. These results are presented in
Figure 3.3-6. The efficiency effect of the approximation error was
determined to be 0.9704 at the high frequency.

3.3.4 Manufacturing, Assembly and Deployment Effects

The effects related to our ability to produce a reflector surface
approaching a zero error wrap rib approximation were evaluated. This
evaluation was based on data developed during manufacturing, assembly
and testing of the ATS-6 flight reflector and therefore should be
reasonably representative of achievable tolerances.

The significant manufacturing error is that of machining the parabolic
contour on the rib. This operation if performed on a precision numeri-
cal control machine can be expected to achieve a final contour accuracy
of 0.051 mm (0.002 inches) RMS. Upon reflector assembly each of the
ribs must be mounted to the hub. Past experience indicates that the
hinge and rib root can be adjusted within ± 0.051 mm (0.002 inches) of
the required position and the rib tips within ± 0.254 mm (0.010 inches).
During reflector deployment the rib locks up with some deployment repeat-
ability error. This error has been measured at ± 0.254 mm (0.010 inches)
at the rib tip for reflectors with rib lengths of 8 to 10 m.

50
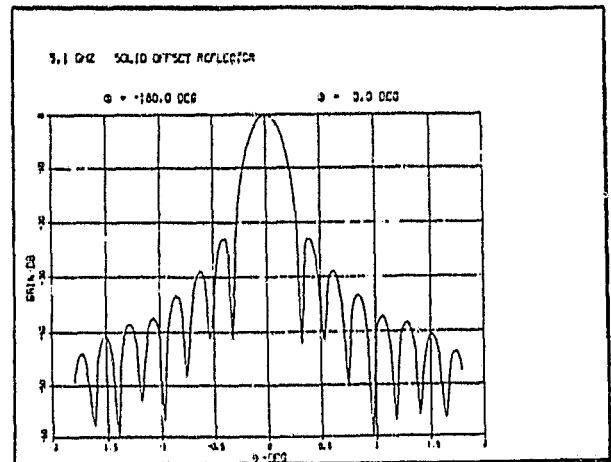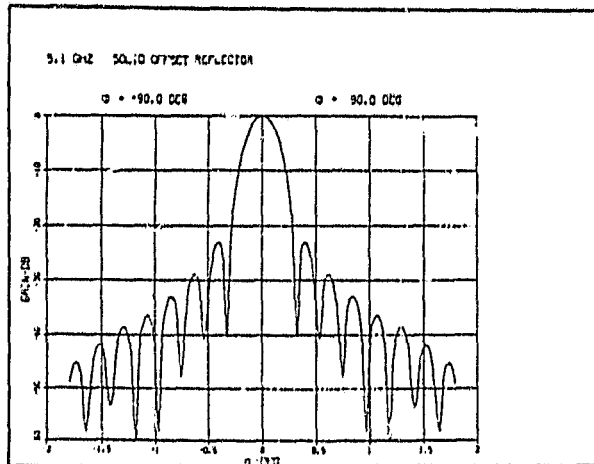
a
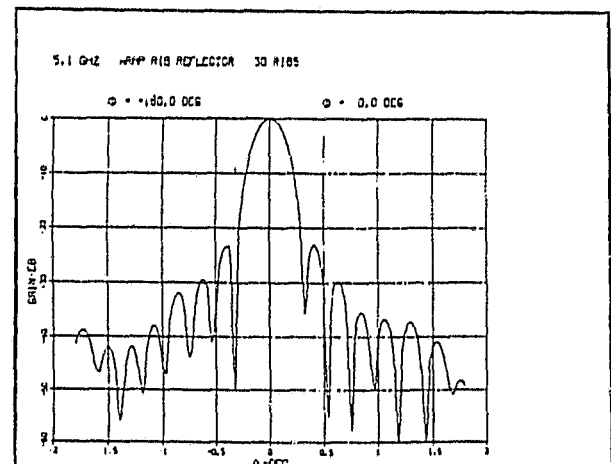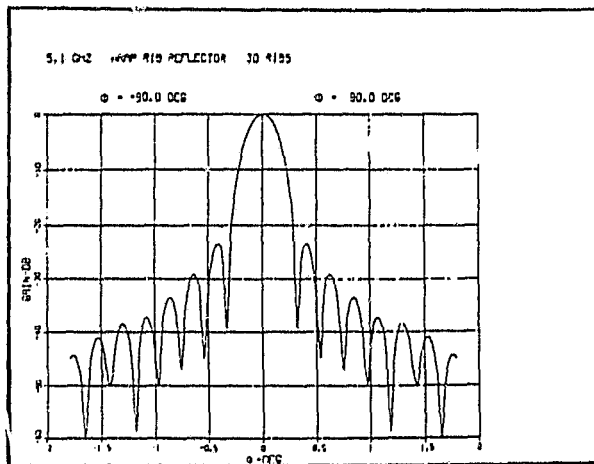
b

Figure 3.3-5 Reflector Pattern Predictions - 5.1 GHz

51
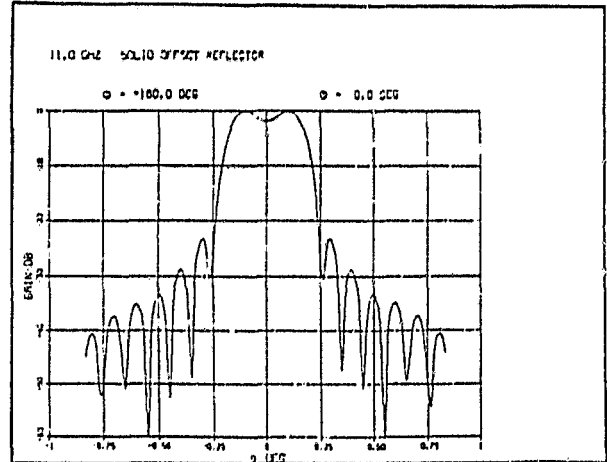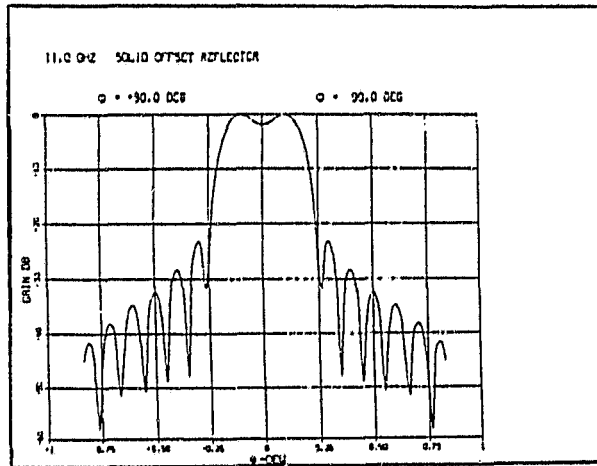
a
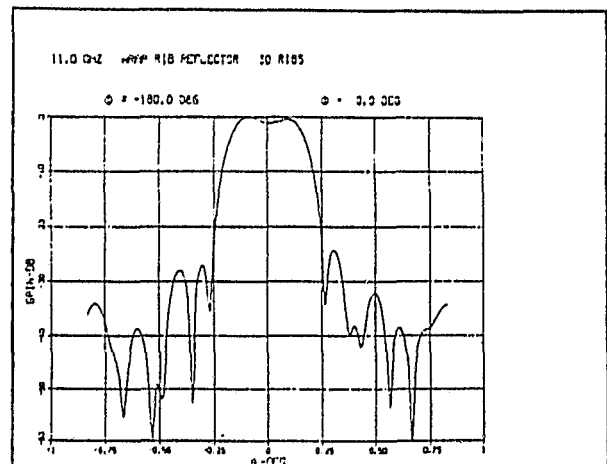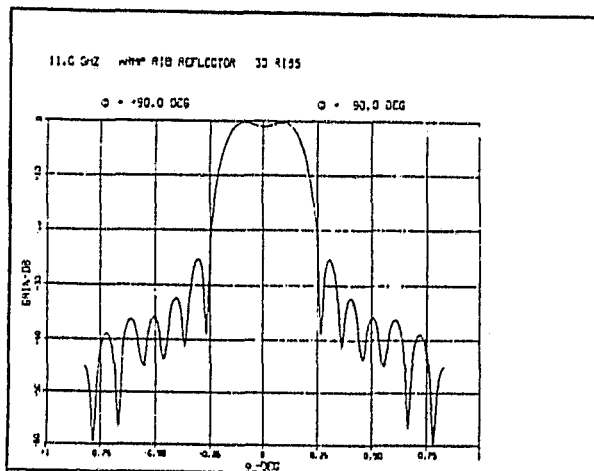
b

Figure 3.3-6   Reflector Pattern Predictions - 11.0 GHz

52

Figure 3.3-7 presents the resulting surface errors and associated aperture efficiencies for the above effects. Since there is no truly accurate method for analytically distributing these errors and achieving a rigorous pattern, the main beam efficiencies are assumed to be equal to the more conservative aperture efficiencies.

3.3.5 Mechanical Scan Effects

The mechanical scan of 6 RPM produces a time invariable load on the reflector support structure and the reflector structure. This loading, being an invariant condition, can be pre-biased out as a source of surface error. However, in doing this it must be realized that spin rate variation must then be assessed as a source of error. In order to evaluate the spin rate variation effects, assumed at $\pm$ 1% of the nominal 6 RPM rate and to define the initial bias shape requirements the reflector was analyzed for the spin induced distortions.

A NEPSAP, Nonlinear Elastic Plastic Structural Analysis Program, finite element model of the 15 M reflector was constructed. The model consisted of 241 modal points and 436 beam and membrane finite elements. This model is displayed in Figure 3.3-8. The ribs were represented as offset beam elements, the mesh as orthotropic membrane elements. The ribs were tapered lenticular elements with dimensions as shown below.

As can be seen from the table, two rib designs were evaluated:

	LOCATION	HEIGHT	WIDTH	THICKNESS
CASE 1	ROOT	177.8 mm	38.1 mm	0.508 mm
	TIP	50.8 mm	12.7 mm	0.508 mm
CASE 2	ROOT	254 mm	38.1 mm	0.508 mm
	TIP	50.8 mm	12.7 mm	0.508 mm

Figure 3.3-7

Manufacturing, Assembly and Deployment Effects

SOURCE	RMS SURFACE ERROR (ε)	
	5.1 GHz	11 GHz
RIB MANUFACTURING	$0.865 \times 10^{-3} \lambda$	$1.318 \times 10^{-3} \lambda$
RIB ROOT ASSEMBLY	$0.611 \times 10^{-3} \lambda$	$1.864 \times 10^{-3} \lambda$
RIB TIP ASSEMBLY	$1.527 \times 10^{-3} \lambda$	$1.208 \times 10^{-3} \lambda$
DEPLOYMENT	$1.527 \times 10^{-3} \lambda$	$1.208 \times 10^{-3} \lambda$
TOTAL RMS SURFACE ERROR	$2.405 \times 10^{-3} \lambda$	$2.847 \times 10^{-3} \lambda$
ASSOCIATED APERTURE EFFICIENCY*	0.9991	0.9987

$$*\eta = e^{-(4\pi\varepsilon)^2}$$

54
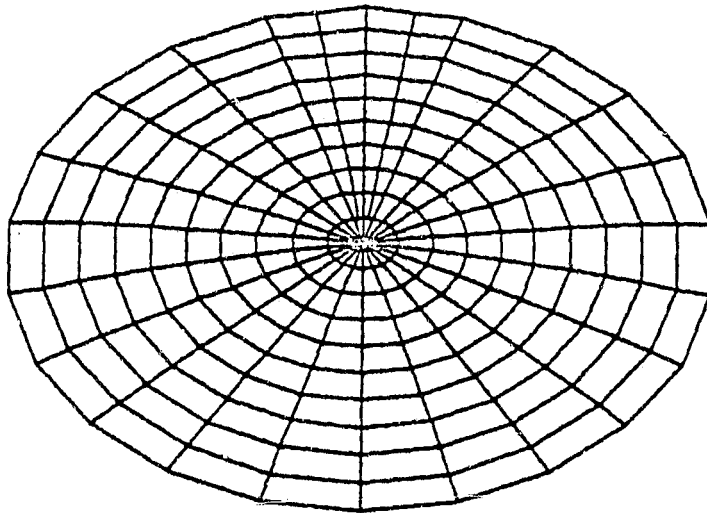
SOLID LINE
UNDEFLECTED ORIGINAL FIGURE
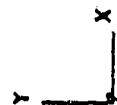
Figure 3.3-8 Structural Model Overview

55

The orthotropic mesh stiffness properties employed in the model were based on ATS-6 mesh values and are defined as:

$$\begin{bmatrix} \text{Radial Line Load (N/mm)} \\ \text{Circumferential Line Load (N/mm)} \\ \text{Shear Line Load (N/mm)} \end{bmatrix} = \begin{bmatrix} 70 & 0 & 0 \\ 0 & 35 & 0 \\ 0 & 0 & 17.5 \end{bmatrix} \times \begin{bmatrix} \text{Radial Strain} \\ \text{Circumferential Strain} \\ \text{Shear Strain} \end{bmatrix}$$

To obtain the 6 RPM reflector distortions, a three increment non-linear analysis was performed. The first increment applied the circumferential mesh prestrain of 0.00088 N/mm (0.005 lb/in). This was then iterated to achieve convergence. The spin loads were then applied to produce the reflector distortions.

Figure 3.3-9 presents a summary of the rib tip deflections of the spin loaded reflector analyzed in Case 1. The developed surface RMS for the 6 RPM condition was calculated to be 30 mm (1.18 in) RMS. This uncompensated error would be unacceptable. Case 2 results, presented in Figure 3.3-10, yield a higher 32 mm (1.27 in) RMS. These results indicate substantial mesh effects due to spin which is consistent with the type of mesh employed. As a result the reflector must be biased for the nominal 6 RPM for weight and spin deflection considerations the lighter Case 1 rib was chosen for use in the design. A spin rate variation of ± 1% of nominal was chosen for the error design requirement.

The effects on efficiency ratioed from the 6 RMP case for a ± 1% spin rate variation yield an 0.3 mm (0.0118 in) RMS surface for the 5.1 GHz case. This provides an aperture efficiency of 0.9959. The 11 GHz under illuminated case has an 0.11 mm (0.0043 in) surface RMS and a corresponding efficiency of 0.9975.

DISU NEP1 1 3 10/240/10

/DISU/NEP1/ 1/ 3/   LIBRARY 17   DIV = 1.000E+00

NODAL DISPLACEMENT TABLE

NODE	INCR	X	Y	Z	XX	YY	ZZ
10	3	1.213E+00	2.189E-03	-1.366E+00	1.160E-05	8.013E-03	-8.592E-06
20	3	1.210E+00	3.953E-02	-1.374E+00	-1.879E-03	7.559E-03	-1.442E-03
30	3	1.325E+00	7.825E-02	-1.533E+00	-4.056E-03	7.174E-03	-2.843E-03
40	3	1.443E+00	1.092E-01	-1.701E+00	-5.767E-03	5.898E-03	-4.354E-03
50	3	1.477E+00	1.314E-01	-1.776E+00	-6.775E-03	3.753E-03	-5.257E-03
60	3	1.450E+00	1.468E-01	-1.777E+00	-7.014E-03	1.367E-03	-5.619E-03
70	3	1.313E+00	1.490E-01	-1.640E+00	-6.210E-03	-8.743E-04	-5.199E-03
80	3	1.103E+00	1.400E-01	-1.410E+00	-4.775E-03	-2.475E-03	-4.216E-03
90	3	8.760E-01	1.211E-01	-1.159E+00	-3.199E-03	-3.313E-03	-3.032E-03
100	3	6.748E-01	9.059E-02	-9.402E-01	-1.800E-03	-3.517E-03	-1.875E-03
110	3	5.380E-01	4.811E-02	-7.947E-01	-7.620E-04	-3.400E-03	-8.589E-04
120	3	4.930E-01	-1.880E-03	-7.489E-01	-4.135E-08	-3.365E-03	-2.527E-06
130	3	5.255E-01	-5.174E-02	-7.733E-01	7.313E-04	-3.303E-03	8.424E-04
140	3	6.573E-01	-9.364E-02	-9.084E-01	1.708E-03	-3.382E-03	1.830E-03
150	3	8.630E-01	-1.235E-01	-1.131E+00	3.083E-03	-3.222E-03	2.988E-03
160	3	1.102E+00	-1.421E-01	-1.398E+00	4.729E-03	-2.460E-03	4.221E-03
170	3	1.316E+00	-1.497E-01	-1.632E+00	6.182E-03	-8.725E-04	5.207E-03
180	3	1.451E+00	-1.455E-01	-1.767E+00	6.980E-03	1.364E-03	5.622E-03
190	3	1.473E+00	-1.279E-01	-1.760E+00	6.733E-03	3.732E-03	5.238E-03
200	3	1.427E+00	-1.026E-01	-1.673E+00	5.648E-03	5.790E-03	4.304E-03
210	3	1.338E+00	-7.149E-02	-1.540E+00	4.034E-03	7.228E-03	2.921E-03
220	3	1.252E+00	-3.442E-02	-1.419E+00	1.926E-03	7.825E-03	1.515E-03
230	3	5.197E+00	1.179E-01	-5.379E-01	0.000E+00	0.000E+00	0.000E+00
240	3	5.315E+00	-1.160E-01	-5.500E-01	0.000E+00	0.000E+00	0.000E+00

Figure 3.3-9   6 RPM Rib Tip Deflections, 178 mm Rib

SU NEP1 1 3 10/240/10

/DISU/NEP1/ 1/ 3/   LIBRARY 17   DIU = 1.000E+00
NODAL DISPLACEMENT TABLE

NODE	INCR	X	Y	Z	XX	YY	ZZ
10	3	1.394E+00	2.441E-03	-1.577E+00	-7.574E-06	8.744E-03	9.053E-06
20	3	1.386E+00	3.985E-02	-1.578E+00	-2.006E-03	8.223E-03	-1.612E-03
30	3	1.450E+00	7.863E-02	-1.678E+00	-4.138E-03	7.377E-03	-2.975E-03
40	3	1.551E+00	1.120E-01	-1.830E+00	-5.862E-03	5.971E-03	-4.413E-03
50	3	1.620E+00	1.398E-01	-1.950E+00	-7.066E-03	3.885E-03	-5.438E-03
60	3	1.618E+00	1.594E-01	-1.984E+00	-7.420E-03	1.445E-03	-5.940E-03
70	3	1.482E+00	1.644E-01	-1.851E+00	-6.657E-03	-9.392E-04	-5.595E-03
80	3	1.254E+00	1.560E-01	-1.603E+00	-5.180E-03	-2.701E-03	-4.606E-03
90	3	1.010E+00	1.362E-01	-1.339E+00	-3.587E-03	-3.720E-03	-3.380E-03
100	3	8.166E-01	1.040E-01	-1.143E+00	-2.197E-03	-4.229E-03	-2.194E-03
110	3	6.799E-01	5.681E-02	-1.006E+00	-9.952E-04	-4.357E-03	-1.074E-03
120	3	6.237E-01	-1.331E-03	-9.469E-01	-3.000E-07	-4.300E-03	-1.218E-06
130	3	6.734E-01	-5.943E-02	-9.947E-01	9.765E-04	-4.305E-03	1.070E-03
140	3	8.117E-01	-1.065E-01	-1.132E+00	2.171E-03	-4.198E-03	2.193E-03
150	3	1.007E+00	-1.381E-01	-1.328E+00	3.539E-03	-3.686E-03	3.363E-03
160	3	1.252E+00	-1.572E-01	-1.593E+00	5.147E-03	-2.689E-03	4.603E-03
170	3	1.482E+00	-1.646E-01	-1.844E+00	6.631E-03	-9.376E-04	5.592E-03
180	3	1.612E+00	-1.578E-01	-1.969E+00	7.372E-03	1.433E-03	5.911E-03
190	3	1.608E+00	-1.362E-01	-1.928E+00	6.977E-03	3.844E-03	5.394E-03
200	3	1.547E+00	-1.076E-01	-1.818E+00	5.798E-03	5.928E-03	4.412E-03
210	3	1.465E+00	-7.492E-02	-1.691E+00	4.167E-03	7.468E-03	3.032E-03
220	3	1.388E+00	-3.553E-02	-1.577E+00	2.010E-03	8.234E-03	1.617E-03
230	3	5.137E+00	1.122E-01	-5.348E-01	0.000E+00	0.000E+00	0.000E+00
240	3	5.170E+00	-1.083E-01	-5.380E-01	0.000E+00	0.000E+00	0.000E+00

Figure 3.3-10 6 RPM Rib Tip Deflections, 254 mm Rib

58

APPENDIX A

SURFACE MODEL

The reflector surface model is being supplied in a NASTRAN compatible data file. This file contains the absolute coordinate locations of 186 reflector surface nodes equally distributed on each of the 30 ribs and mesh gores. Table A-1 presents a listing of the data file over half of the planar symmetric reflector surface. As presented in the table nodes 1 through 6 present surface points for rib 1, the rib which starts at the center of the offset and has a tip closest to the parent reflector vertex. Nodes 7 through 12 present the coordinates of the center of the mesh gore between rib 1 and 2. The sets of 6 nodes then continue to alternate rib and mesh gore nodes through rib 16. Thus displaying 16 ribs and 15 gores.

A right hand coordinate system is used with the origin located at the vertex of the parent parabola. The +Z axis points towards the focal point. The +Y axis is radial from the vertex passing through the offset reflector and is the axis of planar symmetry. All units in this table are in inches.

A-1

NODE NO.	X-CORD	Y-CORD	Z-CORD
1	.000	374.020	39.434
2	.000	241.976	16.490
3	.000	187.297	9.328
4	.000	145.323	5.353
5	.000	109.948	3.270
6	.000	78.732	1.575
7	.000	374.020	39.484
8	13.913	243.459	16.803
9	19.616	189.370	10.268
10	23.968	147.863	6.390
11	27.620	112.869	3.387
12	30.326	82.036	2.262
13	.000	374.020	39.484
14	27.827	244.942	17.116
15	39.232	191.454	10.708
16	47.936	150.403	6.926
17	55.241	115.789	4.504
18	61.652	85.290	2.950
19	.000	374.020	39.484
20	41.072	249.303	18.037
21	57.914	197.596	12.003
22	70.770	157.873	8.505
23	81.562	124.388	6.320
24	91.035	94.371	4.373
25	.000	374.020	39.484
26	54.317	253.665	18.959
27	76.596	203.718	13.239
28	93.604	165.354	10.034
29	107.833	132.397	8.136
30	120.419	104.452	6.397
31	.000	374.020	39.484
32	66.233	260.661	20.435
33	93.483	213.559	15.376
34	114.264	177.356	12.619
35	131.711	146.797	11.052
36	147.032	119.344	10.249
37	.000	374.020	39.484
38	78.248	267.657	21.913
39	110.379	223.393	17.454
40	134.923	139.353	15.153
41	155.539	160.607	13.969
42	173.645	135.236	13.499
43	.000	374.020	39.484
44	88.419	276.917	23.368
45	124.757	236.434	20.207
46	152.527	205.266	18.513
47	175.860	179.922	17.337
48	196.359	155.659	17.812
49	.000	374.020	39.484
50	93.599	286.177	25.324
51	139.135	249.469	22.960
52	170.130	221.175	21.873
53	196.192	197.836	21.705
54	219.074	176.091	22.125
55	.000	374.020	39.484
56	106.568	297.251	28.162
57	150.437	265.074	26.255
58	183.991	240.233	25.897
59	212.204	219.191	26.341
60	237.004	200.576	27.299
61	.000	374.020	39.484
62	114.546	308.326	30.500
63	161.739	280.678	29.550
64	197.851	259.291	29.922
65	228.225	241.145	30.977
66	254.933	225.070	32.471

Table A-1 Reflector Surface Coordinates

LOCKHEED MISSILES & SPACE COMPANY. INC.

67	.000	374.020	39.484	97	.000	374.020	39.484
68	120.050	320.721	33.118	98	131.456	386.551	47.017
69	169.564	298.165	33.242	99	185.961	391.168	52.879
70	207.471	280.666	34.435	100	227.304	394.483	53.466
71	239.370	265.736	36.180	101	263.092	397.124	63.911
72	267.429	252.580	33.279	102	294.191	399.335	69.264
73	.000	374.020	39.484	103	.000	374.020	39.484
74	125.554	333.117	35.735	104	128.792	399.840	43.822
75	177.388	315.651	36.334	105	182.249	409.936	56.951
76	217.091	302.041	39.948	106	223.309	417.552	63.336
77	250.514	290.427	41.394	107	257.952	423.733	69.533
78	279.925	280.090	44.033	108	288.494	429.160	75.560
79	.000	374.020	39.484	109	.000	374.020	39.484
80	128.404	346.326	38.524	110	126.129	413.130	52.628
81	181.472	334.307	40.873	111	178.536	428.803	60.324
82	222.144	324.867	43.768	112	219.314	440.620	68.206
83	256.398	316.762	46.944	113	252.812	450.441	75.166
84	286.552	309.510	50.300	114	282.797	459.986	81.857
85	.000	374.020	39.484	115	.000	374.020	39.484
86	131.253	359.534	41.313	116	120.763	425.675	55.276
87	185.556	352.962	44.812	117	170.990	446.588	64.578
88	227.196	347.692	48.587	118	209.610	462.443	72.812
89	262.292	343.096	52.504	119	242.223	475.680	80.493
90	293.179	338.931	56.512	120	270.995	487.243	87.321
91	.000	374.020	39.484	121	.000	374.020	39.484
92	131.355	373.043	44.165	122	115.358	433.820	57.925
93	185.758	372.065	48.846	123	163.443	464.373	68.333
94	227.500	371.088	53.526	124	200.407	484.266	77.419
95	262.687	370.110	58.207	125	231.533	500.313	85.321
96	293.685	369.133	62.888	126	259.133	515.499	93.735
				127	.000	374.020	39.484
				128	107.437	449.439	60.304
				129	152.276	480.366	71.709
				130	186.749	503.907	81.565
				131	215.331	523.649	90.619
				132	241.601	540.965	99.160

Table A-1 Reflector Surface Coordinates (Continued)

A-3

LOCKHEED MISSILES & SPACE COMPANY, INC.

133	.000	374.020	39.484
134	99.576	460.757	62.652
135	141.109	496.359	75.035
136	173.091	523.549	85.710
137	200.129	546.381	95.416
138	224.008	566.430	104.535
139	.000	374.020	39.484
140	99.388	470.224	64.681
141	136.696	509.808	77.923
142	155.435	540.076	89.198
143	179.739	565.522	99.456
144	201.207	587.886	109.063
145	.000	374.020	39.484
146	79.200	479.691	66.673
147	112.284	523.257	80.762
148	137.780	556.605	92.638
149	159.348	584.663	103.496
150	179.406	609.342	113.591
151	.000	374.020	39.484
152	67.134	486.870	68.195
153	95.190	533.463	82.916
154	116.817	569.156	95.337
155	135.116	599.206	106.565
156	151.287	625.649	117.032
157	.000	374.020	39.484
158	55.067	494.049	69.710
159	78.096	543.670	85.071
160	95.854	591.707	97.985
161	110.883	613.748	109.634
162	124.169	641.956	120.474
163	.000	374.020	39.484
164	41.654	499.536	70.657
165	59.077	550.053	86.418
166	72.514	589.560	99.643
167	83.837	622.950	111.555
168	93.942	652.167	122.628
169	.000	374.020	39.484
170	28.240	503.024	71.604
171	40.053	556.437	87.765
172	49.174	597.413	101.300
173	56.892	631.952	113.476
174	63.716	662.377	124.793
175	.000	374.020	39.484
176	14.120	504.551	71.927
177	20.029	558.610	88.224
178	24.537	600.038	101.865
179	28.446	635.053	114.130
180	31.858	665.855	125.517
181	.000	374.020	39.484
182	.000	506.079	72.249
183	.000	560.784	88.683
184	.000	602.762	102.429
185	.000	638.153	114.784
186	.000	669.334	126.251

Table A-1   Reflector Surface Coordinates (Continued)

A-4